Sangjin Ryu¹

Department of Mechanical and Materials Engineering, Nebraska Center for Materials and Nanoscience, University of Nebraska-Lincoln, W307 Nebraska Hall, Lincoln, NE 68588 e-mail: sryu2@unl.edu

Ethan Davis

Department of Mechanical and Materials Engineering, University of Nebraska-Lincoln, W341D Nebraska Hall, Lincoln, NE 68588 e-mail: ethan.davis@huskers.unl.edu

Jae Sung Park

Department of Mechanical and Materials
Engineering,
University of Nebraska-Lincoln,
W317.2 Nebraska Hall,
Lincoln, NE 68588
e-mail: jaesung.park@unl.edu

Haipeng Zhang

Department of Mechanical and Materials
Engineering,
University of Nebraska-Lincoln,
303 Scott Engineering Center,
Lincoln, NE 68588
e-mail: haipeng.zhang@huskers.unl.edu

Jung Yul Yoo

Fellow ASME
Department of Mechanical Engineering,
Seoul National University,
1 Gwanak-ro, Gwanak-gu,
Seoul 08826, South Korea
e-mail: jyyoo@snu.ac.kr

Wall-Shear-Stress-Based Conditional Sampling Analysis of Coherent Structures in a Turbulent Boundary Layer

Coherent structures are critical for controlling turbulent boundary layers due to their roles in momentum and heat transfer in the flow. Turbulent coherent structures can be detected by measuring wall shear stresses that are footprints of coherent structures. In this study, wall shear stress fluctuations were measured simultaneously in a zero pressure gradient turbulent boundary layer using two house-made wall shear stress probes aligned in the spanwise direction. The wall shear stress probe consisted of two hot-wires on the wall aligned in a V-shaped configuration for measuring streamwise and spanwise shear stresses, and their performance was validated in comparison with a direct numerical simulation result. Relationships between measured wall shear stress fluctuations and streamwise velocity fluctuations were analyzed using conditional sampling techniques. The peak detection method and the variable-interval time-averaging (VITA) method showed that quasi-streamwise vortices were inclined toward the streamwise direction. When events were simultaneously detected by the two probes, stronger fluctuations in streamwise velocity were detected, which suggests that stronger coherent structures were detected. In contrast to the former two methods, the hibernating event detection method detects events with lower wall shear stress fluctuations. The ensemble-averaged mean velocity profile of hibernating events was shifted upward compared to the law of the wall, which suggests low drag status of the coherent structures related with hibernating events. These methods suggest significant correlations between wall shear stress fluctuations and coherent structures, which could motivate flow control strategies to fully exploit these correlations. [DOI: 10.1115/1.4049403]

Introduction

Coherent structures in turbulent boundary layers have been investigated for many years by computational and experimental fluid dynamics research communities [1,2]. The coherent structure or motion is defined as "a three-dimensional region of the flow over which at least one fundamental flow variable exhibits significant correlation with itself or with another variable over a range of space and/or time that is significantly larger than the smallest local scales of the flow" [1]. Various types of coherent structures exist in the turbulent boundary layer, including quasi-streamwise vortices and shear layers in the near-wall region, and transverse vortices in the outer region. These structures are directly related to momentum and heat transfer processes in the turbulent boundary layer as exemplified by quasi-streamwise vortices known to induce high skin-friction regions in turbulent boundary layers [3]. Therefore, recognizing these structures is important in understanding and controlling the turbulent boundary layer for drag reduction or heat transfer augmentation [4-8].

Wall shear stress components manifest turbulent coherent structures because their fluctuations are signatures of turbulence phenomena directly above the wall [9-11]. Therefore, coherent motions can be detected based on wall shear stress [3,12-15]. As such, various techniques have been developed to measure velocity gradients in turbulent boundary layers [16], and some sensors are specialized in measuring wall shear stress [17-19]. Among such sensors, surface-mounted thermal sensors have been in wide use to measure wall shear stress based on heat transfer from the sensor to the flow [20–22]. While the heated sensing element of these thermal sensors is subjected to fluid flow, the convective heat loss from the heated element to the flow increases as fluid flow past the element and thus shear stress increase. This heat transfer rate can be converted into an electrical signal, and the relationship between shear stress and the electrical signal of the thermal sensor can be determined via calibration. To measure streamwise wall shear stress, the thermal sensors are arranged with its long axis being perpendicular to the streamwise direction. In the case of spanwise wall shear stress, one or two thermal sensors are aligned in parallel with respect to the streamwise direction [23]. For simultaneous measurement of the both quantities, two sensors are arranged in a V configuration with the bisector pointing to the streamwise direction [24–28]. In addition to the traditional thermal sensor, various wall shear stress measurement techniques

¹Corresponding author.

Contributed by the Fluids Engineering Division of ASME for publication in the JOURNAL OF FLUIDS ENGINEERING. Manuscript received August 4, 2020; final manuscript received December 16, 2020; published online January 22, 2021. Assoc. Editor: Timothy Lee.

have been developed based on optical diagnostics and microelectromechanical system (MEMS) fabrication [17,21,22,29,30].

Coherent structures have been experimentally studied based on correlation and conditional sampling between the wall shear stress and velocity components measured in the boundary layer. Based on a correlation between wall shear stress and streamwise velocity fluctuations in a turbulent channel flow, Eckelmann found that wall shear stress fluctuations lagged behind streamwise velocity fluctuations [31]. Blackwelder and Eckelmann measured streamwise and spanwise velocity components and their wall-normal gradients, and found that pairs of counter-rotating streamwise vortices occurred frequently in the wall region of a bounded turbulent shear flow [32]. From simultaneous measurements of fluctuating velocity components and their gradients at the wall in a turbulent channel flow, Kreplin and Eckelmann deduced that coherent structures inclining toward the streamwise direction traveled downstream [33]. Alfredsson et al. measured wall shear stress fluctuations with various methods in various flow media, and showed a correlation between wall shear stress and streamwise velocity [34]. They also suggested that the intensities of streamwise and spanwise wall shear stress fluctuations were 0.4 and 0.2, respectively. Wietrzak and Lueptow analyzed a detailed relation between wall shear stress and streamwise velocity fluctuations in an axisymmetric boundary layer [35]. They showed that transverse curvature had little effect on the near-wall burst-sweep cycle, and that the tilting angle of a turbulent structure correlated with wall shear stress was 18 deg. Using a direct numerical simulation (DNS) database, Kravchenko et al. showed that high wall shear stress values were directly associated with streamwise vortices very close to the wall and suggested that these vortices tilted by 6 deg from the streamwise direction [3]. Based on simultaneous measurements of wall shear stress and streamwise velocity fluctuations, Yang et al. found that wall shear stress was highly correlated with turbulent structures tilting from the wall in the streamwise direction [36]. Osterlünd et al. performed similar simultaneous measurements in high-Reynolds-number turbulent boundary layers using a MEMS-type hot-film sensor array and detected tilted coherent structures in a turbulent boundary

In this study, we simultaneously measured wall shear stresses using two V-shaped wall shear stress probes and near-wall streamwise velocity fluctuations using a hot-wire probe in a zero pressure gradient turbulent boundary layer. Each of the two wall shear stress probes could measure streamwise and spanwise wall shear stress components simultaneously, and they were arranged sideby-side in the spanwise direction [38,39]. The hot-wire probe was placed between the two wall shear stress probes and moved upward and downstream, to investigate relationships between fluctuations in wall shear stresses and streamwise velocity as a function of their streamwise and vertical distances. Previously, we analyzed turbulent coherent structures highly correlated with wall shear stress fluctuations based on correlations between wall shear stress and streamwise velocity [39]. In contrast, this study employed three different conditional sampling methods: the peak detection method, the variable-interval time-averaging (VITA) method, and the hibernating event detection method, to detect coherent structures correlated with wall shear stress fluctuations. More importantly, wall shear stress fluctuations simultaneously measured by the two shear stress probes were used for simultaneous event detection for the peak detection method and the VITA method.

Methods

Wind Tunnel and Turbulent Boundary Layer. An open circulation subsonic wind tunnel was used in this study, where the bottom of the test section $(3.6 \,\mathrm{m}\,\log\times0.43 \,\mathrm{m}\,\mathrm{wide}\times0.28 \,\mathrm{m}$ high) was a smooth flat duralumin plate on which a boundary layer developed (Fig. 1(a)). Installed right after the test section

inlet, steel wire and sand paper tripped the boundary layer. The side walls of the test section were adjusted to obtain a zero pressure gradient turbulent boundary layer. Experiments were conducted at free stream velocity (U_{∞}) of 8 m/s. Free stream turbulence intensity and nonuniformity were lower than 0.25% and 0.4% at U_{∞} = 5 m/s, respectively.

Two wall shear stress probes were arranged side-by-side symmetrically with respect to the centerline of the bottom plate at $2.9 \,\mathrm{m}$ downstream from the test section inlet (Fig. 1(a)). At the measurement point, boundary layer thickness (δ) was 57.2 mm, momentum thickness (θ) was 5.9 mm, friction velocity (u_{τ}) was 0.3059 m/s, and Reynolds number values based on momentum thickness and friction velocity were 3,170 and 1,170, respectively. The skin-friction coefficient (C_f) measured at the measurement point with a Preston tube [40] (2.93×10^{-3}) agreed with the law of the wake (3.06×10^{-3}) [41]. Measurement with the Preston tube and Patel's calibration formula [40,42] showed that the spanwise variation of u_{τ} was less than 3% in $-2 < z/\delta < 2$, where z represents the spanwise direction (Fig. 1(a)). Along with static pressure coefficient distribution, this friction velocity distribution confirmed that the developed turbulent boundary layer was twodimensional at the measurement point.

Wall Shear Stress Measurement

V-Type Wall Shear Stress Probes. Arranged in the spanwise direction, two lab-built wall shear stress probes were used to simultaneously measure wall shear stresses in the streamwise and spanwise directions (Figs. 1(a) and 1(b)) [38]. The body of the probe was machined from MC Nylon, and ground while installed to the bottom of the test section, to remove any gaps or steps between the probe body and the duralumin plate. After the probe body was separated from the test section bottom, four 0.3-mm-diameter holes were drilled on the probe body. Then, 0.25-mm-diameter metal prongs for hot-wire were inserted through the holes using a microscope and a microstage with a resolution of $1~\mu m$ and glued to the probe body. After hot-wires were welded to the prongs, the finished probe was installed in the test section.

Each probe consisted of four prongs and two 2.5- μ m-diameter hot-wires that were symmetric with respect to the sensor axis. The normal direction of each wire formed an angle of α with respect to the streamwise direction (Fig. 1(c)). The streamwise and spanwise dimensions of the sensor were 0.4 mm and 1.3 mm, respectively. The length of each wire was about 0.56 mm ($l^+=12$), and therefore its aspect ratio was 226. The hot-wires were 30-50 μ m above the wall ($y^+=0.6$ -1.1), which prevented direct heat conduction to the wall. The axes (bisectors) of the two probes were 2 mm apart from each other ($\Delta z^+=42.9$) [38].

Each hot-wire of the wall shear stress probes was connected to a constant temperature anemometer (Dantec Streamline), and the resistance overheat ratio $(R_w - R_o)/R_o$ was set to 0.3, where R_w and R_o are the operating resistance and cold resistance of the hotwire, respectively [4,35]. Standard square wave test gave frequency responses of 26-30 kHz. Prior to each measurement, the wall shear stress probes were calibrated using the following fourth-order polynomial as a calibration formula:

$$\bar{\tau}_{W,\text{eff}} = C_0 + C_1 \bar{E} + C_2 \bar{E}^2 + C_3 \bar{E}^3 + C_4 \bar{E}^4$$
 (1)

where $\bar{\tau}_{W,\text{eff}}$ is the effective mean streamwise wall shear stress measured using the Preston tube and Patel's calibration formula (Figure S1 available in the Supplementary Materials on the ASME Digital collection) [40,42], \bar{E} is the mean anemometer output voltage of each wire, and C_i 's (i=0-4) are calibration constants for each wire. Therefore, two sets of C_i 's were obtained for each probe, and Eq. (1) enabled converting the output voltage of hot-wires to streamwise wall shear stress.

Wall Shear Stress Calculation. Streamwise and spanwise wall shear stresses $(\tau_{Wx}$ and $\tau_{Wz})$ are

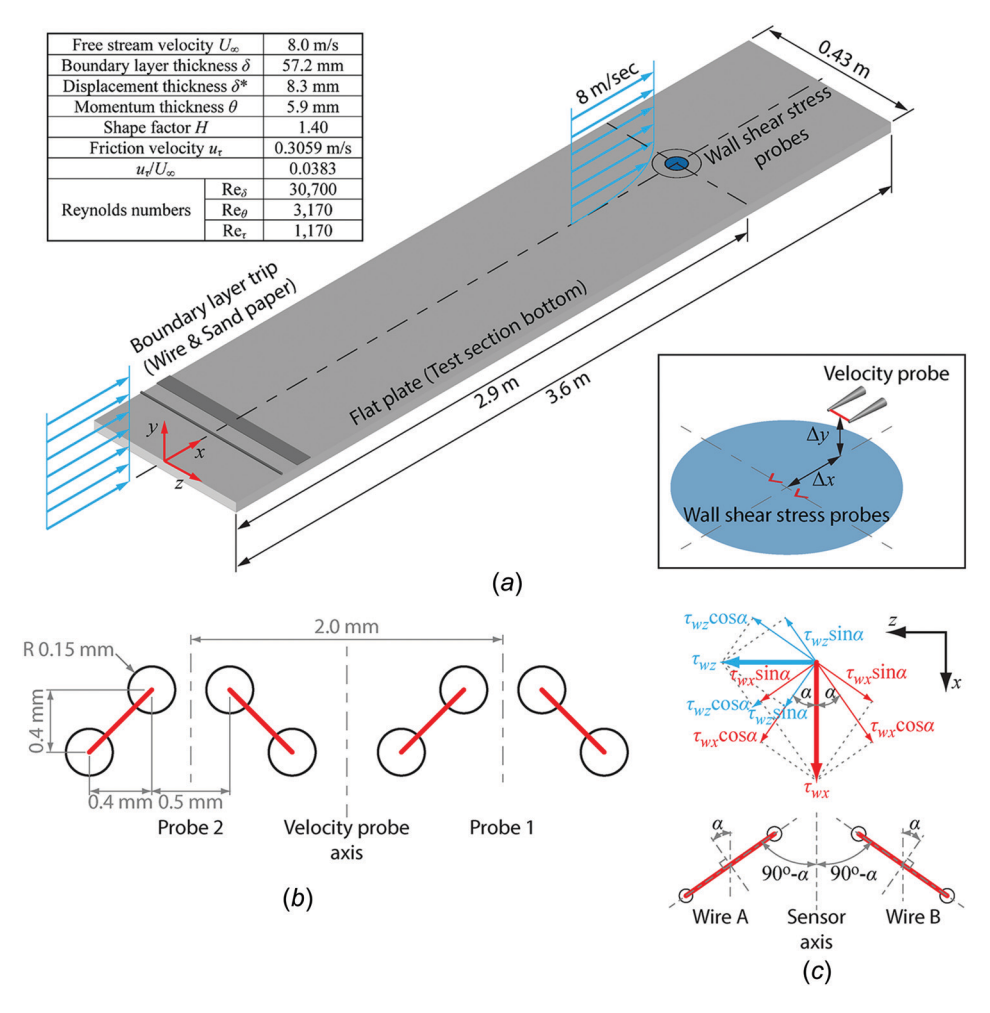


Fig. 1 Experimental setup. (a) Wind tunnel test section. Insets: boundary layer parameters at the wall shear stress measurement location (top) and probe arrangement (bottom). (b) Dimension of the V-type wall shear stress probe array. The hot-wires of the wall shear stress probes are shown in red. (c) Decomposition of wall shear stress vectors.

$$\tau_{Wx} = \mu \frac{\partial u}{\partial y} \bigg|_{y=0} \tag{2a}$$

$$\tau_{Wz} = \mu \frac{\partial w}{\partial y} \bigg|_{y=0} \tag{2b}$$

where u and w are streamwise and spanwise velocities, respectively, y represents the binormal direction (Fig. 1(a)), and μ is the dynamic viscosity of a working fluid. As shown in Fig. 1(c), wall shear stress vectors are decomposed into components parallel and normal to hot-wires according to the geometrical configuration of the wall shear stress probe. The effective wall shear stresses of hot-wires A and B (Fig. 1(c)) are

$$\left(\tau_W^A\right)^2 = \left(\tau_{Wx}\cos\alpha - \tau_{Wz}\sin\alpha\right)^2 + k^2\left(\tau_{Wx}\sin\alpha + \tau_{Wz}\cos\alpha\right)^2 \tag{3a}$$

and

$$(\tau_W^B)^2 = (\tau_{Wx}\cos\alpha + \tau_{Wz}\sin\alpha)^2 + k^2(\tau_{Wx}\sin\alpha - \tau_{Wz}\cos\alpha)^2$$
(3b)

where k is a constant accounting for the effect of heat transfer due to wall shear stress acting parallel to the wire. The analytic solutions of Eq. (3) are [38]

$$\tau_{Wx} = \frac{\sqrt{m+n} + \sqrt{m-n}}{2\sqrt{(1-k^2)\sin 2\alpha[(1+k^2) + (1-k^2)\cos 2\alpha]}}$$
(4a)

$$\tau_{Wz} = \pm \frac{\sqrt{m+n} - \sqrt{m-n}}{2\sqrt{(1-k^2)\sin 2\alpha \left[(1+k^2) - (1-k^2)\cos 2\alpha \right]}}$$
(4b)

where

$$m = [(\tau_W^A)^2 + (\tau_W^B)^2]^2 (1 - k^2) \sin 2\alpha$$
 (5)

and

$$n = |(\tau_W^A)^2 - (\tau_W^B)^2| \sqrt{(1+k^2)^2 - (1-k^2)^2 \cos^2 2\alpha}$$
 (6)

In Eq. (4b), $\tau_{Wz} > 0$ when $\tau_W^A < \tau_W^B$. In the present study, α was approximated to be 45 deg based on the probe geometry, and k was assumed to be 0.2 [43].

Streamwise Velocity Measurement. An I-type hot-wire probe (diameter: $2.5 \,\mu\text{m}$, length: $0.7 \,\text{mm}$ [l^+ =15], resistance overheat ratio: 0.5, frequency response: $37 \,\text{kHz}$) was used to measure the streamwise velocity. The probe satisfied a general criterion for aspect ratio ($l/d = 280 \geq 200$) [44]. Prior to each measurement, the velocity probe was calibrated with respect to free stream

velocities measured with a Pitot tube using a fourth-order polynomial, similar to Eq. (1). The initial distance from the probe to the wall was determined by fitting the measured mean velocity data against the universal law of the wall.

The velocity probe was connected to the same anemometer as the two wall shear stress probes, so that voltage outputs from the anemometer had been sampled for 30 s at a sampling rate of 5 kHz using a 16-bit A/D converter DT2838. Therefore, sampling time interval was $0.2\,\mathrm{ms}$ ($\Delta t^+ = \Delta t u_\tau^2/\nu = 1.22$). For simultaneous measurements of wall shear stress and streamwise velocity, the velocity probe was moved to four different streamwise spots ($\Delta x^+ = 0$, 32, 64, 96) with respect to the wall shear stress probe along the centerline between two wall shear stress probes (Fig. 1(a)).

Conditional Sampling. For detailed investigation of coherent structures, three conditional sampling techniques were employed: the peak detection method [3,35,45], the VITA method [46], and the hibernating event detection method [47–51]. These methods required a detection function to identify significant events from a detection signal, and an "event" was defined as a part of the signal in which the value of the detection function was unity consecutively.

Peak Detection Method. The peak detection method detects events of high-amplitude peaks in a fluctuating signal Q'. Applied to velocity or wall shear stress signals, the peak detection method identifies intense turbulence events [35]. The detection function for Q' is defined as

$$D_{\text{peak}}(t) = \begin{cases} 1, & \text{if } |Q'(t)| > k_{\text{peak}}Q_{\text{rms}} \\ 0, & \text{otherwise} \end{cases}$$
 (7)

where $k_{\rm peak}$ is the threshold level for peak detection, and Q_{rms} is the root-mean-square (rms) value of Q'. In addition to the detection function, the sign of Q' is used as an additional detection criterion. When Q'>0 and $D_{\rm peak}=1$, events are identified to be positive peak events, and vice versa. When the positive detection criterion is applied to τ'_W , the peak detection method identifies significant increases in τ'_W .

VITA Method. It is known that the VITA method can identify moments of significant turbulence generation [46]. The VITA method requires the short-time variance var calculated by

$$\operatorname{var}(t,T) = \frac{1}{T} \int_{t-T/2}^{t+T/2} Q'^{2}(s) ds - \left[\frac{1}{T} \int_{t-T/2}^{t+T/2} Q'(s) ds \right]^{2}$$
 (8)

where T is the averaging time. Then, the detection function is defined as

$$D_{\text{VITA}}(t) = \begin{cases} 1, & \text{if var} > k_{\text{VITA}} Q_{\text{rms}}^2 \\ 0, & \text{otherwise} \end{cases}$$
 (9)

where $k_{\rm VITA}$ is the threshold level. In addition, the VITA method employs the time gradient of the fluctuating signal $(\partial Q'/\partial t)$ when an event occurs. Depending on whether the gradient is positive or negative, the event is called the positive or negative VITA event, respectively. When these detection criteria are applied to u', the VITA method identifies significant instantaneous acceleration (positive event) or deceleration (negative event) of flow.

Ensemble Averaging for the Peak Detection and VITA Method. After events were detected from the signal using the peak detection method or VITA method, the "wholesale scheme" of Murlis et al. [52] was applied to the detected events. If the time difference between two neighboring events was smaller than $10\nu/u_\tau^2$, which corresponded to about 8 sampling intervals, the two events

were merged into one event [45]. Then, conditional average was calculated by

$$\langle Q(t_{cs})\rangle = \frac{1}{N} \sum_{i=1}^{N} Q'(t_i + t_{cs})$$
 (10)

where t_i is the event detection time of the i-th event, t_{cs} is the ensemble average time span with respect to t_i , and N is the number of detected events. The event detection time t_i was defined as the time of the largest peak in peak events, and the midpoint of VITA events, respectively. Then, obtained $\langle Q \rangle$ was normalized with $k_{\rm peak}^{1/2}Q_{\rm rms}$ for the peak detection method, and $k_{\rm VITA}^{1/2}Q_{\rm rms}$ for the VITA method, respectively, which was denoted by $\langle Q \rangle^*$ [46].

After the conditional average was obtained, phase jitter among detected events was removed. When the detection and data signals are measured simultaneously at different positions in the boundary layer, the conditional average can be affected by a random phase between the two signals [53]. The effect of phase jitter can be reduced by adjusting the event detection time based on the cross-correlation between the conditional average and fluctuating signals in a certain time window with respect to the detection time [54]. For this purpose, the process of detection time adjustment and conditional average calculation was iterated until the cross-correlation was maximized [35,45,55]. The cross-correlation was calculated in the time window of $51\nu/u_{\tau}^2$ [35], and the phase jitter removal process was iterated twice.

Hibernating Event Detection Method. The hibernating event detection method is a recently developed conditional sampling method to investigate the features of stochastic flow cycles between high and low drag intervals based on wall shear stress [47–51]. Based on the level of drag, flow features are classified into high- or low-drag class. The low-drag class is termed "hibernation" [47]. During hibernation, flow fields are relatively less agitated, and the vortical motions are significantly suppressed, which causes low Reynolds shear stress and increases bulk velocity. In this study, a hibernating event was defined as an event when the instantaneous wall shear stress remained lower than 90% of the mean wall shear stress for $t^* = tu_\tau/\delta = 3$, i.e., three eddy turnover times [47,50,51].

Result and Discussion

Turbulence Statistics

Streamwise Velocity. Turbulence statistics were measured in the near-wall region of the formed turbulent boundary layer. Figure 2(a) shows that the measured profile of mean streamwise velocity (U^+) agreed with the universal law of the wall and previous results based on DNS [56] and hot-wire measurement [57]. Therefore, the boundary layer was confirmed to be fully developed at the measurement point. In the vicinity of the wall $(y^+ < 3)$, however, heat transfer from the probe toward the wall increased U^+ .

Fully developed turbulent boundary layer was also confirmed based on streamwise turbulence intensity near the wall; the rms value of u' normalized with friction velocity $(u_{\rm rms}^+ = u_{\rm rms}/u_{\tau})$ agreed with previous results (Fig. 2(b)) [56,57]. The maximum of $u_{\rm rms}^+$ is known to be independent of the Reynolds number within statistical errors, and its most probable value is 2.71 ± 0.14 for turbulent boundary layers [58], which our case satisfied $(u_{\rm rms}^+|_{\rm max} = 2.80)$.

Wall Shear Stress. The performance of the wall shear stress probes was validated by comparing it with previous experimental and computational studies [38]. A DNS study of a turbulent channel flow suggested little correlation between the instantaneous streamwise (τ_{Wx}) and spanwise (τ_{Wz}) components of wall shear stress (Fig. 3(*a*)) [59]. Our measurement of τ_w also confirmed this observation (Figs. 3(*b*) and 3(*c*)). Compared with the DNS result, however, the

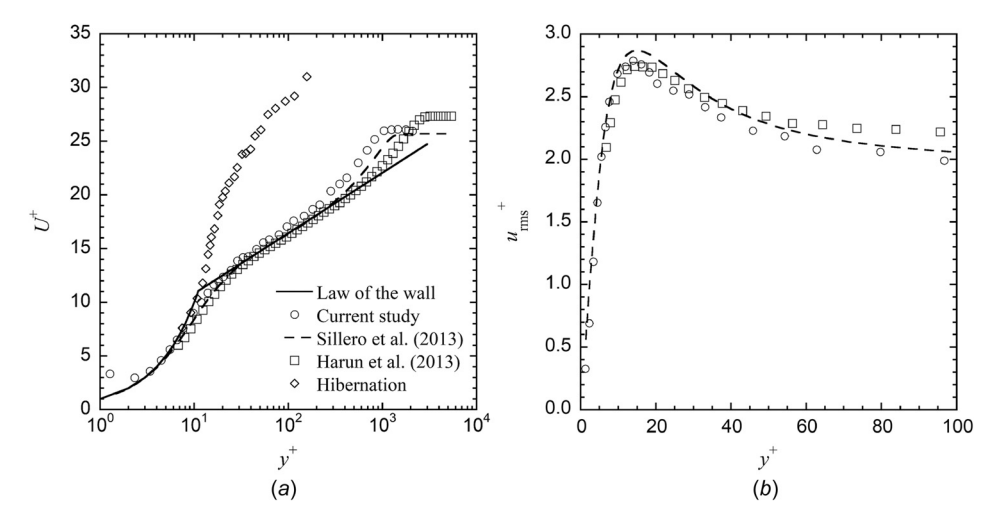


Fig. 2 Streamwise velocity measurement of the turbulent boundary layer. (a) Mean velocity profiles including one for ensemble-averaged hibernating events. (b) Turbulence intensity profiles. The hot-wire measurement of the current study is compared with the DNS result of Sillero et al. (Re $_{\tau}$ = 2780-6680) [56] and experimental measurement of Harun et al. (Re $_{\tau}$ \approx 3000) [57].

measured distribution of τ_{Wx} showed less dispersion and higher density. In addition, the rms angle of measured τ_w with respect to the streamwise direction was 8.9 deg for Probe 1 and 8.0 deg for Probe 2 whereas that of the simulation result was 12.4 deg.

One reason for these differences is that hot-wires for wall shear stress measurement were slightly raised from the wall ($y^+ \approx 1$) to reduce heat transfer to the wall, and thus the probes actually measured τ_w slightly above the wall. Another reason is that the wall shear stress probes could measure τ_w only when it lied within ± 45 deg with respect to the *x*-direction due to its configuration. However, the contribution of the second reason seems negligible because the DNS result showed that the number of such cases was less than 1% of the whole data [59].

The turbulence intensity of τ_w ($I_i = \tau_{Wi,rms}/\bar{\tau}_{Wx}$ where i=x or z) was affected by the effective length of the sensing hot-wire. I_x and I_z were measured to be 0.21 and 0.16, respectively. Repeated measurements (N=10) of I_x and I_z showed uncertainty of 1.1% and 1.5% for 95% confidence [38]. The value of I_x is known to vary in a wide range (0.06-0.40) possibly due to the low spatial and temporal resolutions of used sensors, heat loss to the substrate, and different fluid media [34,35]. Although our measurement of I_x belonged to this range, it was lower compared to previous results of similar Re ranges (DNS result of Kim et al.

[60]: 0.36 at $\text{Re}_{\tau} = 180$, and hot-wire measurement of Wietrzak and Lueptow [35]: 0.32 at $\text{Re}_{\theta} = 3050$). This difference could be caused by assumed values for α and k, and possible asymmetry between two hot-wires of the wall shear stress probes. However, a comparison of the energy spectra of τ'_{Wx} with previous results appeared satisfactory (Fig. S2, Supporting Information) [21]. Also, the energy spectra of τ'_{Wx} and τ'_{Wz} agreed well with each other in the high frequency range, while the energy of τ'_{Wz} was lower than that of τ'_{Wx} in the low-frequency range.

The spanwise dimension of the probe was responsible for the low intensity of τ_{Wx} (Fig. 1(*b*)): although the spanwise dimension of each wire was 0.4 mm, the whole width of the probe was 1.3 mm ($L_z^+=27$). To test the effect of the spanwise dimension of the probe, I_x was measured with each hot-wire of the wall shear stress probe being positioned normal to the flow. Then, I_x increased to 0.29-0.32, which is in agreement with the measurement of Wietrzak and Lueptow [35]. In contrast to L_z^+ , the streamwise dimension of the probe ($L_x^+=8$) was small enough, and thus our measurement of I_z was close to the DNS result of Kim et al. (0.19 at Re $_{\tau}=180$) [60].

Conditionally Averaged Peak Event. Since the performance of the peak detection method depends on the threshold level [45],

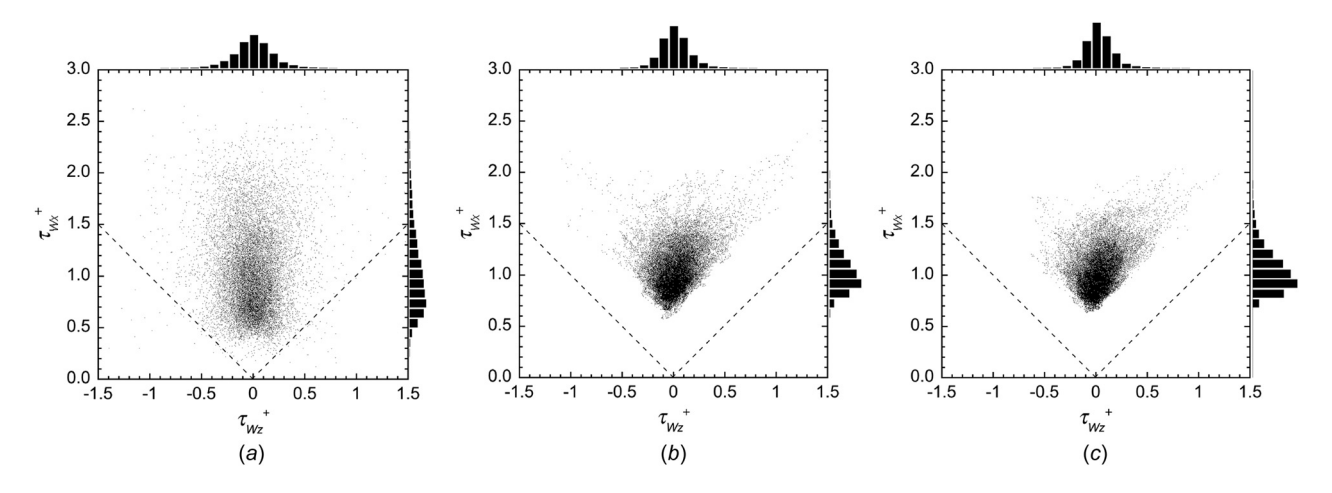


Fig. 3 Scatter plots of instantaneous wall shear stress vectors (τ_{Wx} : streamwise component, τ_{Wz} : spanwise component). Histograms on the top and right side of each plot show the probability distribution of measured wall shear stress vectors. (a) DNS result of a turbulent channel flow [59]. (B, C) Current results measured with Probe 1 and Probe 2.

we investigated the effect of $k_{\rm peak}$ on the conditionally sampled peak events of τ_W . As $k_{\rm peak}$ increased, the number of the detected events ($N_{\rm peak}$) decreased exponentially for both τ_{Wx} and τ_{Wz} , except negative events of τ_{Wx} (Figs. S3A and S3B). This exponential decrease was previously observed for τ_{Wx} [45], and the same tendency was found for τ_{Wz} in this study. Decreasing $N_{\rm peak}$ means that larger fluctuations were detected less frequently with larger $k_{\rm peak}$. When normalized with $k_{\rm peak}^{1/2}$, the maximum amplitude of $\langle \tau_W \rangle^*$ appeared similar regardless of $k_{\rm peak}$ (Fig. S4), which means that the maximum amplitude of $\langle \tau_W \rangle$ increased with $k_{\rm peak}$. Thus, $k_{\rm peak} = 1$ was used for the following analyses. It is also noted that the two probes agreed well with each other in terms of $\langle \tau_W \rangle^*$.

Figure 4(a) shows an example of conditionally averaged positive events $(k_{\text{peak}} = 1)$. The detection signal was u measured at $\Delta x^+ = 0$ and $y^+ = 7.3$, and conditionally averaged u and τ_W were normalized with their respective rms values. The sign of $\langle \tau_{Wz1} \rangle^*$ was negative while the sign of $\langle \tau_{Wz2} \rangle^*$ was positive, which suggests that the wall shear stress probes sensed a pair of streamwise vortices which caused sweep and burst in the near wall region. When sweep occurred, u' was positive, and τ'_{Wz1} and τ'_{Wz2} became negative and positive, respectively (Fig. 4(b)). In contrast, the sign of $\langle \tau_{Wx} \rangle^*$ was positive for both probes. These differences in sign between the wall shear stress components were also confirmed with the space–time correlation between τ'_W and u' [39]. It is also apparent that there were time differences between the peaks of $\langle u \rangle^*$ and $\langle \tau_{Wz} \rangle^*$: the peak event of u' preceded that of τ'_{Wz} at $\Delta x^+ = 0$. This phase shift shows that coherent structures correlated with wall shear stress were inclined, which was observed in the time-averaged space-time correlation [36,39].

Changes in u' upon significant fluctuations of τ'_W were investigated by applying the peak detection method to τ'_W and then obtaining $\langle u \rangle^*$ at various y^+ positions. Since sweep events were related to positive τ'_{Wx} , negative τ'_{Wz1} and positive τ'_{Wz2} as explained in Fig. 4, u' was averaged with respect to peak events of $\tau'_{Wx1} > 0$ or $\tau'_{Wx2} > 0$ (the first row in Figs. 5 and S5A), or peak events of $\tau'_{Wz1} < 0$ or $\tau'_{Wz2} > 0$ (the second row in Figs. 5 and S5A). As shown by the top two rows of Fig. 5, positive u' was associated with sweep events, and phase shift existed between $\langle u \rangle^*$ and $\langle \tau_W \rangle^*$ in terms of the time of the peak amplitude. The peak of $\langle u \rangle^*$ always preceded those of $\langle \tau_W \rangle^*$ (i.e., $t_{cs}^+ = 0$) for $\Delta x^+ = 0$, and the peaks of $\langle u \rangle^*$ moved in the positive t_{cs}^+ direction as Δx^+ increased. As a result, at $\Delta x^+ = 96$, some peaks of $\langle u \rangle^*$ lagged behind that of $\langle \tau_W \rangle^*$. This suggests that a streamwise

vortex, which is correlated with instantaneous large fluctuations of wall shear stress, inclines toward the streamwise direction [45].

The peak detection method was also applied for burst events. Since burst events were related to negative τ'_{Wx} , positive τ'_{Wz1} and negative τ'_{Wz2} , which is opposite to the sweep event, u' was averaged with respect to peak events of $\tau'_{Wx1} < 0$ or $\tau'_{Wx2} < 0$ (the third row in Figs. 5 and S5A), or peak events of $\tau'_{Wz1} > 0$ or $\tau'_{Wz2} < 0$ (the fourth row in Figs. 5 and S5A). As shown by the bottom two rows of Fig. 5, negative u' was associated with burst events. It was noted that the peak magnitudes of $\langle \tau_{Wx} \rangle^*$ in burst events were lower than those in sweep events (Fig. S5A), which suggests that fluctuations in τ_{Wx} were stronger for sweep events than for burst events. This difference is also supported by the asymmetric distribution of τ'_{Wx} shown in Fig. 3. The peak magnitudes of $\langle u \rangle^*$ in burst events were lower than those in sweep events similarly, and $\langle u \rangle^*$ curves of burst events were less smooth and showed less dependence on y⁺ than those of sweep events. In contrast, the peak magnitudes of $\langle \tau_{Wz} \rangle^*$ in burst events were similar to those in sweep events (Fig. S5A), which is supported by the symmetric distribution of τ'_{Wz} shown in Fig. 3. In contrast to $\langle u \rangle^*$ associated with $\tau'_{Wx} < 0$, $\langle u \rangle^*$ curves associated with τ'_{Wz} in burst events showed clearer dependence on y⁺ and looked similar to those in sweep events. Similar to sweep events, phase shift existed in burst events.

To test whether wall shear stress probes sensed the same flow structure, we used both τ'_W signals measured by the two probes (Fig. 6). Fewer peak events were detected when the simultaneous peak detection was applied (Fig. S3C), but exponential decrease was also observed. This reduction in the event number seems to have been caused by mismatch between the fixed probe spacing and the variable vortex-to-vortex spacing, as well as by the existence of single vortices not forming vortex pairs. For sweep events (Fig. 6(a)), an event was detected only when positive τ'_{Wx} events occurred on both probes simultaneously, or when events of $\tau'_{Wz1} < 0$ and $\tau'_{Wz2} > 0$ occurred simultaneously (Fig. S5B). Although phase jitter was not removed, $\langle u \rangle^*$ based on the simultaneous peak detection showed larger peaks compared to $\langle u \rangle^*$ shown in Fig. 5. A similar trend was observed for burst events simultaneously occurring on the two probes (Fig. 6(b)). This suggests that the wall shear stress probes did not always detect the same flow structure, and that when they did, stronger fluctuations occurred in streamwise velocity. It is well accepted that streamwise vortices do not always exist in a pair in the turbulent

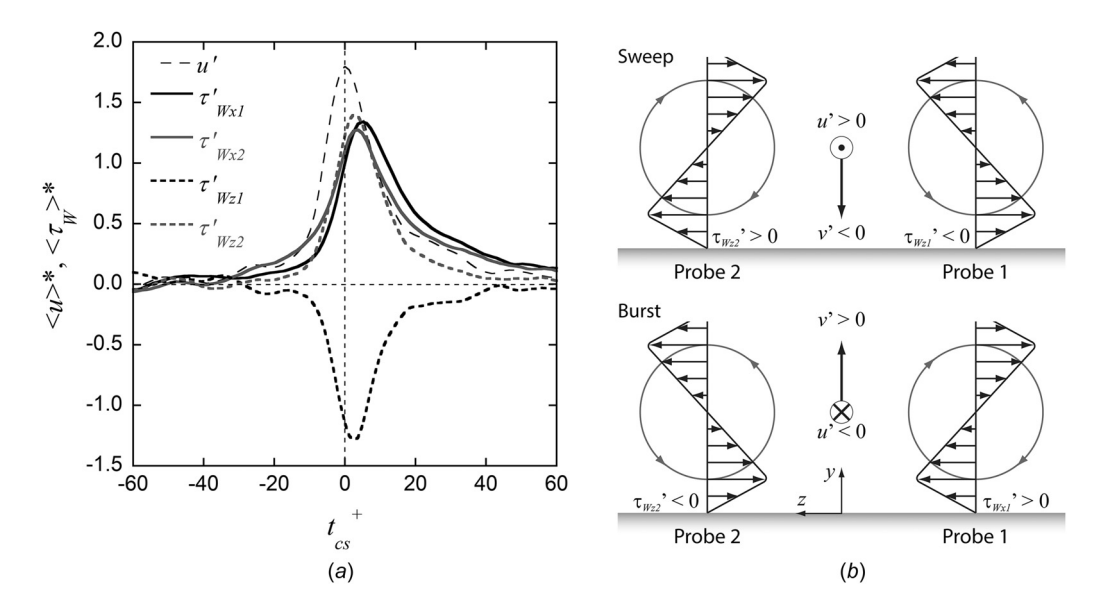


Fig. 4 Conditionally averaged peak events. (a) The detection signal ($k_{\rm peak}=1$) was streamwise velocity measured at $y^+=7.3$ and $\Delta x^+=0$. (b) Schematic diagram of the streamwise vortex pair sensed by the wall shear stress probes.

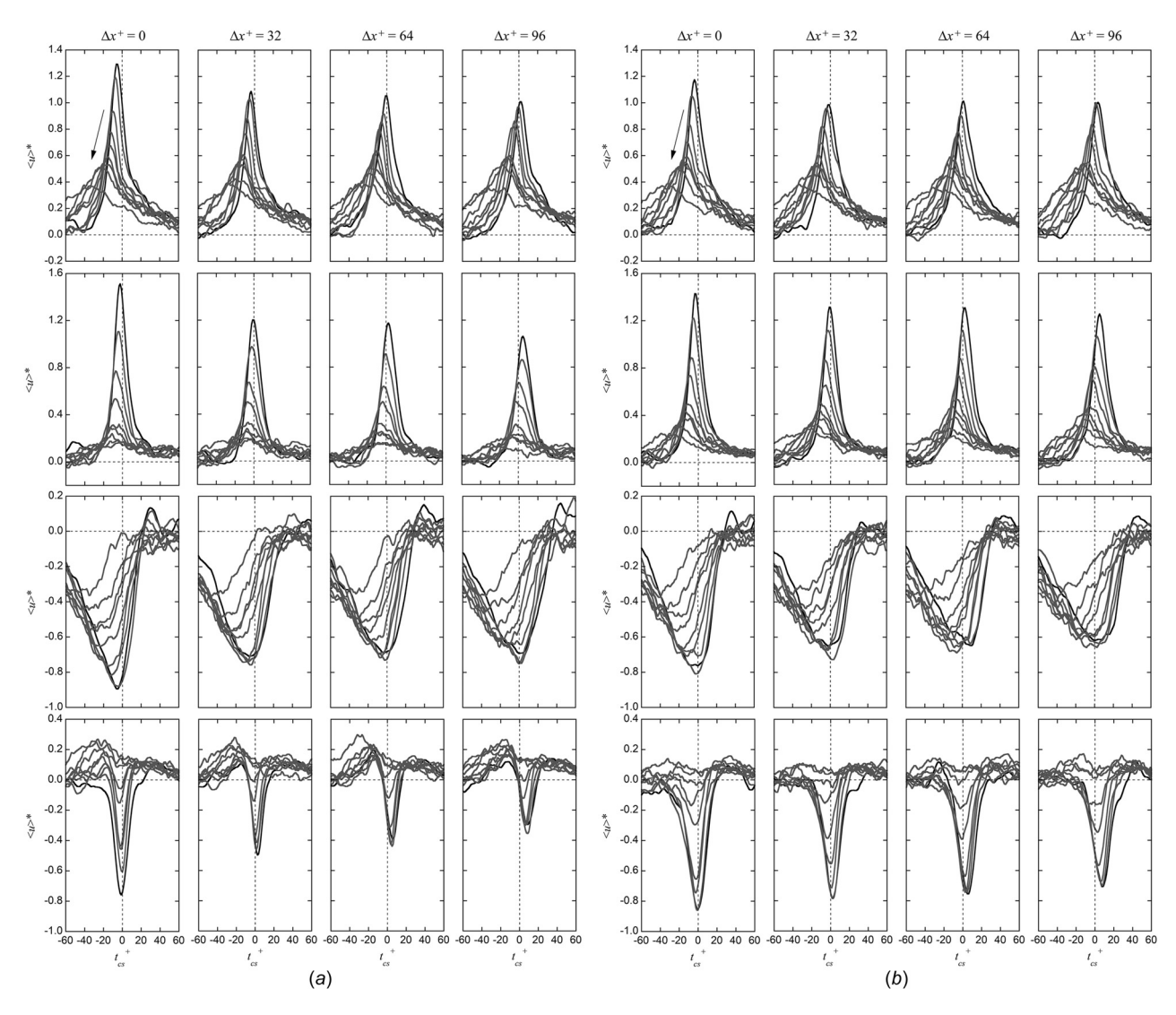


Fig. 5 Conditionally averaged streamwise velocity fluctuations $\langle u \rangle^*$ with respect to the peak events of wall shear stress ($k_{\text{peak}} = 1$; Fig. S5A). (a) Probe 1. (b) Probe 2. The top two rows are for sweep events, and the bottom two for burst events. The arrow indicates the direction of increasing y^+ : $y^+ = 7.3$, 10.5, 16.0, 21.3, 34.3, 51.8, 69.2, 103.9, and 173.5, and $\langle u \rangle^*$ curves of $y^+ = 7.3$ are shown in black.

boundary layer [61], which supports our simultaneous peak detection results

Conditionally Averaged VITA Event. Similarly to the peak detection method, the performance of the VITA method depends on both k_{VITA} and T [62,63]. The number of detected events of τ_W decreased exponentially with increasing $k_{\rm VITA}$ while it increased with increasing T^+ (= Tu_τ^2/ν) (Fig. S6). Although k_{VITA} values affect the performance of the VITA method, it is known that conditional average results show little dependence on k_{VITA} when normalized with $k_{\text{VITA}}^{1/2}Q_{\text{rms}}$ [46]. As such, $\langle \tau_W \rangle^*$ curves showed little dependence on k_{VITA} values (Fig. S7A). Since the normalization involves $k_{\rm VITA}^{1/2}$ as a denominator, agreement among $\langle \tau_W \rangle^*$ curves suggests that $\langle \tau_W \rangle$ showed more rapid temporal changes as k_{VITA} increased. In regard to the effect of T^+ , the VITA method is known to detect events lasting roughly for the averaging time, and thus it filters out fluctuating signals with slower changes as T^+ increases [63]. $\langle \tau_W \rangle^*$ showed greater amplitude as T^+ decreased (Fig. S7B), which suggests that instantaneous large fluctuations in τ_W were related to high frequency components of $\tau'_W[45]$.

Figure 7 shows examples of conditionally averaged VITA events. The detection signal was u measured at $\Delta x^+ = 0$ and

 $y^+=7.3$. It is notable that for the positive event of $\langle u \rangle^*$, which corresponds to the sweep event, $\langle \tau_{Wz1} \rangle^*$ showed the negative event while $\langle \tau_{Wz2} \rangle^*$ showed the positive event. The opposite behavior of $\langle \tau_{Wz} \rangle^*$ was observed for the negative event of $\langle u \rangle^*$, which is the burst event. Similar to the conditionally averaged peak event shown in Fig. 4(a), the observed opposite sign between $\langle \tau_{Wz1} \rangle^*$ and $\langle \tau_{Wz2} \rangle^*$ supports the existence of the streamwise vortex pair (Fig. 4(b)). In contrast, the event sign of $\langle \tau_{Wx} \rangle^*$ was always the same as that of $\langle u \rangle^*$ regardless of the wall shear stress probes because $\tau'_{Wx} \approx \mu u'/\Delta y$. It is also notable that there were time differences between the inflection points of $\langle u' \rangle$ and $\langle \tau'_{Wz} \rangle$: the VITA event of u' preceded that of τ'_{Wz} , which shows the existence of the inclined coherent structure correlated with wall shear stress [36,39].

Changes in u' upon significant changes in τ'_W were investigated by applying the VITA method to τ'_W and then obtaining $\langle u \rangle^*$ at various y^+ positions. Since sweep events were related to positive τ'_{Wx} , negative τ'_{Wz1} and positive τ'_{Wz2} as explained in Fig. 4, u' was averaged with respect to positive VITA events of τ'_{Wx1} or τ'_{Wx2} (the first row in Figs. 8 and S8A), or negative VITA events of τ'_{Wz1} or positive VITA events of τ'_{Wz1} (the second row in Figs. 8 and S8A). As shown by the top two rows of Fig. 8, the temporal increase in u' was associated with sweep events, and phase shift

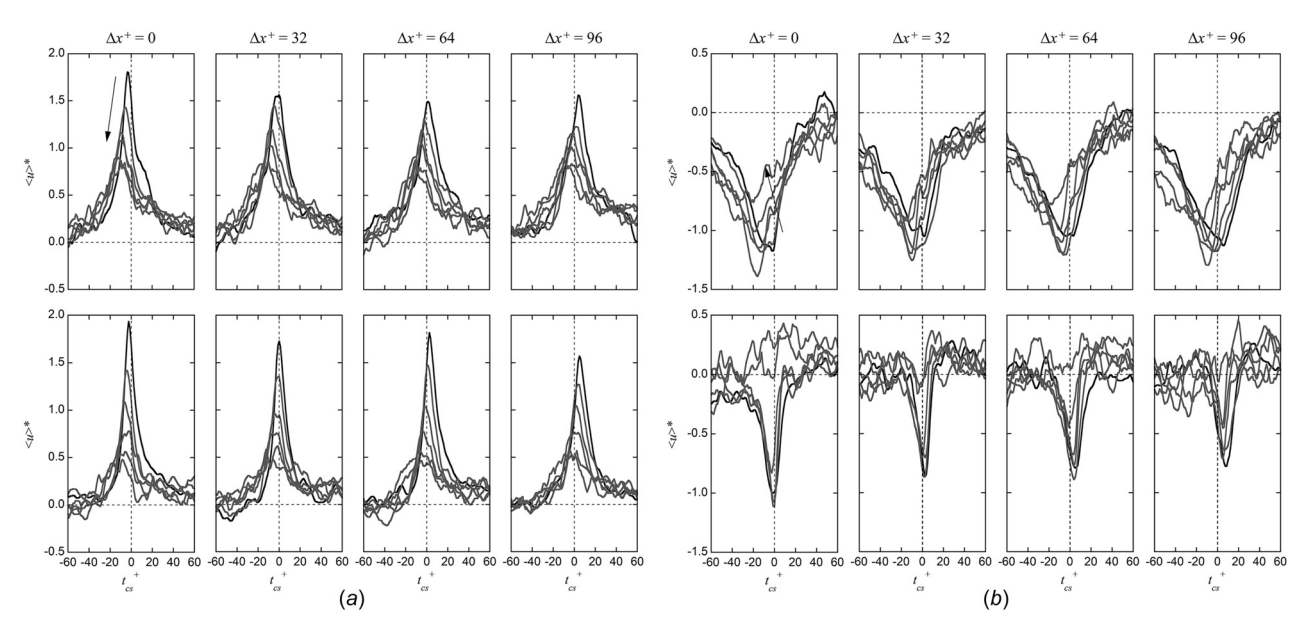


Fig. 6 Conditionally averaged streamwise velocity fluctuations $\langle u \rangle^*$ with respect to the simultaneous peak events of wall shear stress ($k_{\text{peak}} = 1$; Fig. S5B). (a) Sweep events. (b) Burst events. The arrow indicates the direction of increasing y^+ : $y^+ = 7.3$, 10.5, 16.0, 21.3, 34.3, and 51.8, and $\langle u \rangle^*$ curves of $y^+ = 7.3$ are shown in black.

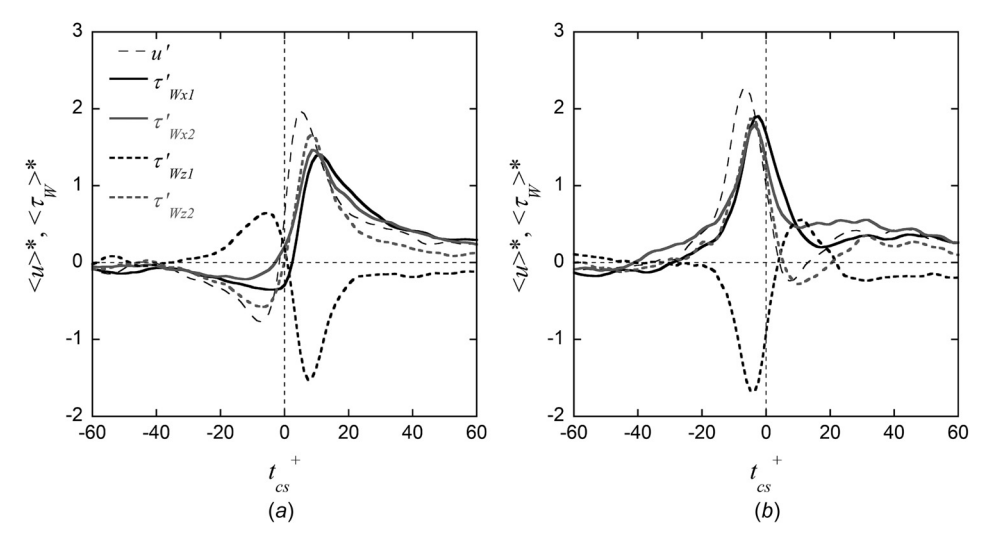


Fig. 7 Conditionally averaged VITA events ($k_{\text{VITA}} = 1$, $T^+ = 16$). The detection signal was streamwise velocity measured at $y^+ = 7.3$ and $\Delta x^+ = 0$. (a) Positive event. (b) Negative event.

existed between $\langle u \rangle^*$ and $\langle \tau_{Wz} \rangle^*$ in terms of the time of the maximum gradient or inflection point. The inflection points of $\langle u \rangle^*$ always preceded those of $\langle \tau_{Wz} \rangle^*$ (i.e., $t_{cs}^+ = 0$) for $\Delta x^+ = 0$, and moved in the positive t_{cs}^+ direction as Δx^+ increased, which is similar to the peak detection results. This suggests that a streamwise vortex, which is correlated with temporal gradient of wall shear stress, inclines toward the streamwise direction [45], which agrees with the peak detection results.

The VITA method was also applied for burst events. Since burst events were related to negative τ'_{Wx} , positive τ'_{Wz1} and negative τ'_{Wz2} , which is opposite to the sweep event, u' was averaged with respect to negative VITA events of τ'_{Wx1} or τ'_{Wx2} (the third row in Figs. 8 and S8A), or positive VITA events of τ'_{Wz1} or negative VITA events of τ'_{Wz2} (the fourth row in Figs. 8 and S8A). As shown by the bottom two rows of Fig. 8, temporal decrease in u' was associated with burst events.

Similar to the peak detection method, simultaneous event detection was tried with the VITA method (Fig. 9). For sweep events (Fig. 9(a)), an event was detected when positive VITA events of

 τ'_{Wx} occurred on both probes simultaneously, or when a negative VITA event of τ'_{Wz1} and a positive VITA event of τ'_{Wz2} occurred simultaneously (Fig. S8B). Although phase jitter was not removed, $\langle u \rangle^*$ based on the simultaneous VITA event detection showed more rapid changes in $\langle u \rangle^*$ compared to the top two rows of Fig. 8. A similar trend was observed for burst events simultaneously occurring on the two probes (Fig. 9(b)). This result suggests that when the wall shear stress probes detected VITA events of the same sign simultaneously, streamwise velocity increased or decreased more rapidly.

Conditionally Averaged Hibernating Event. The hibernating events were detected using one of the two wall shear stress probes and the aforementioned criteria. As shown in Fig. 10(a), the criteria for the hibernating event were satisfied in terms of wall shear stress and time duration. The fraction of time spent in hibernation was observed to be about 0.02, where we detected more than 70 hibernating events for $t^+ = 7.36 \times 10^6$. The fluctuations of

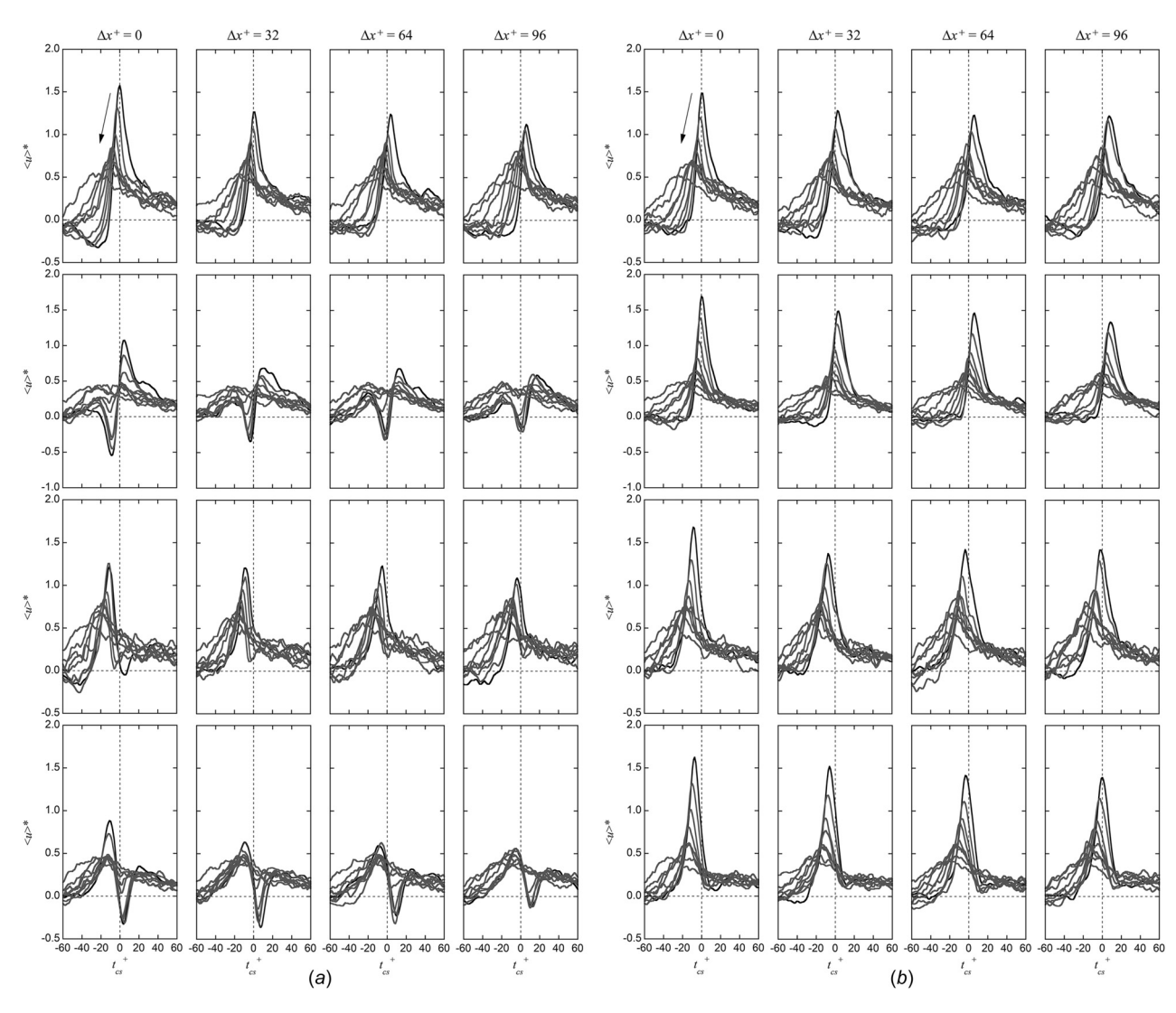


Fig. 8 Conditionally averaged streamwise velocity fluctuations $\langle u \rangle^*$ with respect to the VITA events of wall shear stresses ($k_{\text{VITA}} = 1$, $T^+ = 16$; Fig. S8A). (a) Probe 1. (b) Probe 2. The top two rows are for sweep events, and the bottom two for burst events. The arrow indicates the direction of increasing y^+ : $y^+ = 7.3$, 10.5, 16.0, 21.3, 34.3, 51.8, 69.2, 103.9, and 173.5, and $\langle u \rangle^*$ curves of $y^+ = 7.3$ are shown in black.

streamwise velocity during hibernating events at a given y⁺ were slightly lower than the mean at that given location (Fig. S9), but their behavior was not exactly the same as that of wall shear stress. Figure 2(a) shows the ensemble-averaged mean streamwise velocity profile for hibernation at $\Delta x^+ = 32$, along with profiles for the experimental measurement and the law of the wall. All profiles collapse well in the viscous sublayer ($y^+ \le 5$) and start deviating from the $U^+ = y^+$ line in the buffer layer. The conditional mean velocity profile (i.e., hibernation profile) is shifted upward when compared to the law of the wall. This increase in U^{+} implies a greater bulk velocity, suggesting comparatively lower skin friction or resistance to the flow, during the hibernating events. To our best knowledge, hibernation events are first observed in a turbulent boundary layer and even in high Reynolds number flows of $Re_{\tau} = O(10^3)$. This hibernation profile is similar to that of recent experiments and simulations in channel flow as shown in Fig. 10(*b*) [49,50].

Conclusion

Detecting coherent structures is crucial in understanding the turbulent boundary layer as illustrated by the direct impact of quasi-streamwise vortices on skin friction of the flow, and wall shear stress fluctuations manifesting turbulent coherent structures. In this study, simultaneous measurements of stream- and spanwise wall shear stresses and streamwise velocity fluctuations were carried out in a near-wall turbulent boundary layer using two V-type wall shear stress probes and an I-type hot-wire probe. The wall shear stress probes were fabricated with hot-wires on the wall, and they were validated by comparing their instantaneous wall shear stress measurements with a direct numerical simulation result. Conditional sampling methods were employed to investigate the relationship between wall shear stress and streamwise velocity fluctuations. The peak detection method and the VITA method showed that quasi-streamwise vortices, which are correlated with large fluctuations of wall shear stress, inclined toward the streamwise direction. In particular, conditionally sampled fluctuations of streamwise velocity were stronger when they were simultaneously detected by the two wall shear stress probes than when detected by only one probe. This suggests that when the wall shear stress probes detected the same flow structure, stronger fluctuations occurred in streamwise velocity. The hibernating event detection method showed that the conditional mean velocity profile is shifted upward in comparison with the law of the wall, which suggests lower skin friction during the hibernating events. Therefore, this study could describe how coherent structures are highly

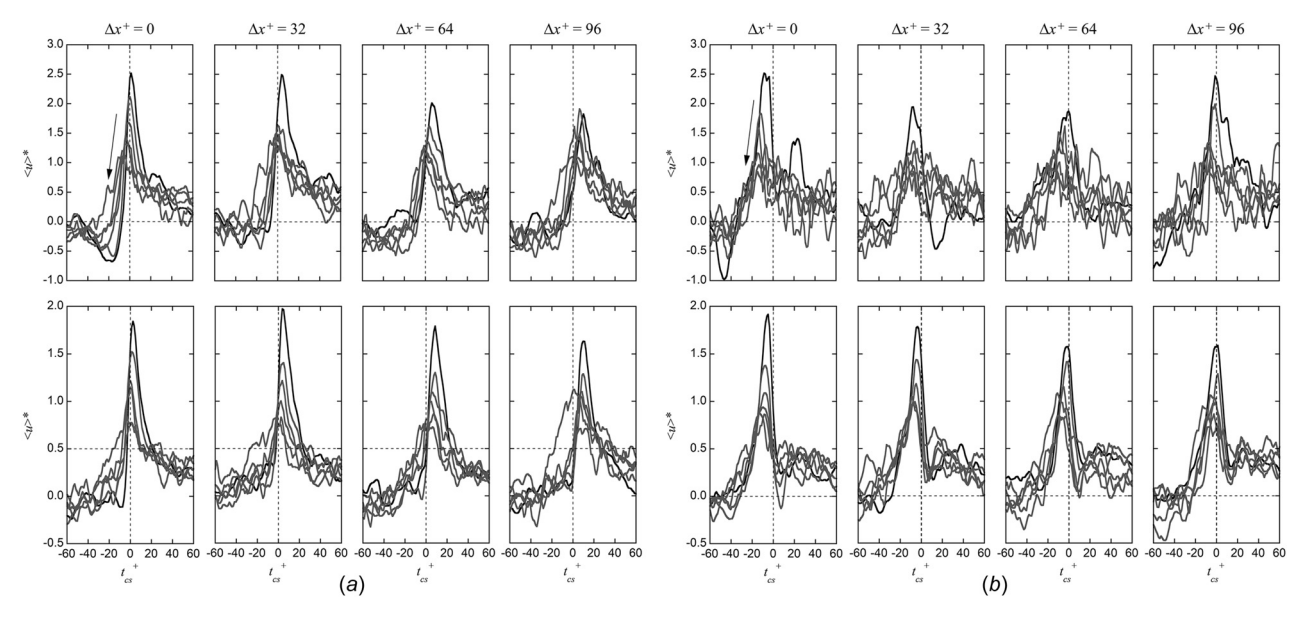


Fig. 9 Conditionally averaged streamwise velocity fluctuations $\langle u \rangle^*$ with respect to the simultaneous VITA events of wall shear stress ($k_{\text{VITA}} = 1$, $T^+ = 16$; Fig. S8B). (a) Sweep events. (b) Burst events. The arrow indicates the direction of increasing y^+ : $y^+ = 7.3$, 10.5, 16.0, 21.3, 34.3, and 51.8, and $\langle u \rangle^*$ curves of $y^+ = 7.3$ are shown in black.

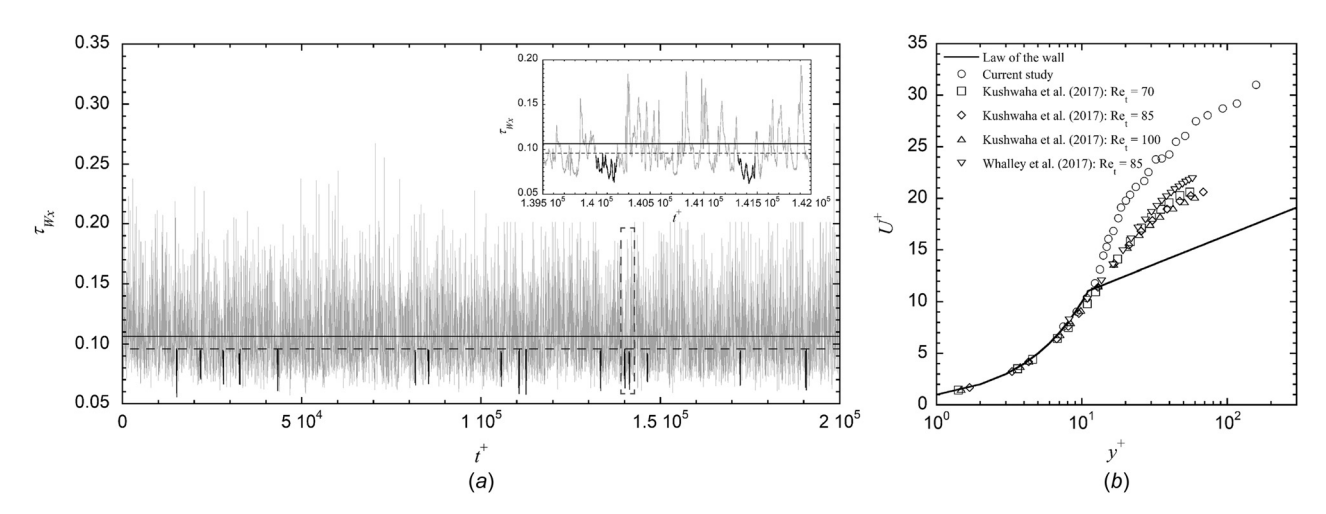


Fig. 10 Hibernating events. (a) Temporal fluctuation of streamwise wall shear stress (gray curve) with identified hibernating events (black curves). Solid line: time-averaged wall shear stress. Dashed line: 90% of the mean value. Inset: A magnified plot of the dashed box area. (b) The mean velocity profile for hibernating events of the current study is compared to the simulation result of Kushwaha et al. [50] and the experimental result of Whalley et al. [49].

correlated with wall shear stress fluctuations in a zero pressure gradient turbulent boundary layer flow, which may suggest important implications for turbulent flow control. For instance, as illustrated herein, hibernation events exhibit uncharacteristically low skin friction relative to the mean behavior of the system. Therefore, controlling the frequency and/or duration of these events presents a favorable target for various flow control methods—e.g., increased number of events or longer duration events for increased drag reduction. The different mechanisms associated with various flow control methods may also have distinct effects on the spatiotemporal characteristics of these events. As such, further investigation is needed to elucidate the effects of turbulent flow control methods on hibernation events.

Acknowledgment

E. A. D. and J. S. P. gratefully acknowledge the financial support in part from the National Science Foundation through a grant OIA-1832976.

Funding Data

• National Science Foundation (No. OIA-1832976).

References

- Robinson, S. K., 1991, "Coherent Motions in the Turbulent Boundary Layer," Annu. Rev. Fluid Mech., 23(1), pp. 601–639.
- [2] Alfonsi, G., 2006, "Coherent Structures of Turbulence: Methods of Eduction and Results," ASME Appl. Mech. Rev., 59(6), pp. 307–323.
- [3] Kravchenko, A. G., Choi, H., and Moin, P., 1993, "On the Relation of Near-Wall Streamwise Vortices to Wall Skin Friction in Turbulent Boundary Layers," Phys. Fluids A, 5(12), pp. 3307–3309.
- [4] Bushnell, D. M., and Henfer, J. N., 1990, Viscous Drag Reduction in Boundary Layer (Progress in Astronautics and Aeronautics), AIAA, Reston, VA.
- [5] Choi, H., Moin, P., and Kim, J., 1994, "Active Turbulence Control for Drag Reduction in Wall-Bounded Flows," J. Fluid Mech., 262, pp. 75–110.
- [6] Kim, J., 2003, "Control of Turbulent Boundary Layers," Phys. Fluids, 15(5), pp. 1093–1105.
- [7] Jiménez, J., 2013, "Near-Wall Turbulence," Phys. Fluids, 25(10), p. 101302.
- [8] Kaithakkal, A. J., Kametani, Y., and Hasegawa, Y., 2020, "Dissimilarity Between Turbulent Heat and Momentum Transfer Induced by a Streamwise Travelling Wave of Wall Blowing and Suction," J. Fluid Mech., 886, p. A29.

- [9] Kline, S. J., Reynolds, W. C., Schraub, F. A., and Runstadler, P. W., 1967, "The Structure of Turbulent Boundary Layers," J. Fluid Mech., 30(4), pp. 741-773.
- [10] Waleffe, F., 1997, "On a Self-Sustaining Process in Shear Flows," Phys. Fluids, 9(4), pp. 883-900.
- [11] Adrian, R. J., 2007, "Hairpin Vortex Organization in Wall Turbulence," Phys. Fluids, 19(4), p. 041301.
- [12] Ge, M.-W., Xu, C.-X., and Cui, G.-X., 2011, "Detection of Near-Wall Streamwise Vortices by Measurable Information at Wall," J. Phys. Conf. Ser., 318, p. 022040.
- [13] Ge, M.-W., Xu, C.-X., and Cui, G.-X., 2015, "Active Control of Turbulence for Drag Reduction Based on the Detection of Near-Wall Streamwise Vortices by Wall Information," Acta Mech. Sin., 31(4), pp. 512-522.
- [14] He, G., Jin, G., and Yang, Y., 2017, "Space-Time Correlations and Dynamic Coupling in Turbulent Flows," Annu. Rev. Fluid Mech., 49(1), pp. 51–70.
- [15] Wang, L., Huang, W., Xu, C., Shen, L., and Zhang, Z., 2019, 'Relationship Between Wall Shear Stresses and Streamwise Vortices,' Appl. Math. Mech., 40(3), pp. 381-396.
- [16] Wallace, J. M., and Vukoslavčević, P. V., 2010, "Measurement of the Velocity Gradient Tensor in Turbulent Flows," Annu. Rev. Fluid Mech., 42(1), pp. 157-181.
- [17] Naughton, J. W., and Sheplak, M., 2002, "Modern Developments in Shear-
- Stress Measurement," Prog. Aerosp. Sci., 38(6–7), pp. 515–570.
 [18] Sun, G., Park, H., and Kim, C.-J., 2015, "Development of a Miniature Shear Sensor for Direct Comparison of Skin-Friction Drags," J. Microelectromech. Syst., 24(5), pp. 1426–1435.
- [19] Xu, M., Arihara, B., Tong, H., Yu, N., Ujiie, Y., and Kim, C. J., 2020, "A Low-Profile Wall Shear Comparator to Mount and Test Surface Samples," Exp. Fluids, 61, pp. 1–13.
- [20] Haritonidis, J. H., 1989, "The Measurement of Wall Shear Stress," Advances in Fluid Mechanics Measurements, Springer, Berlin, pp. 229–261.
 [21] Löfdahl, L., and Gad-el-Hak, M., 1999, "MEMS Applications in Turbulence
- and Flow Control," Prog. Aerosp. Sci., 35(2), pp. 101–203.

 [22] Kuo, J. T. W., Yu, L., and Meng, E., 2012, "Micromachined Thermal Flow Sensors—a Review," Micromachines, 3(3), pp. 550–573.

 [23] Hanratty, T. J., and Campbell, J. A., 1996, "Measurements of Wall Shear
- Stress," Fluid Mechanics Measurements, Taylor and Francis, Philadelphia, PA. [24] Sirkar, K. K., and Hanratty, T. J., 1970, "The Limiting Behavior of the Turbu-
- lent Transverse Velocity Component Close to a Wall," J. Fluid Mech., 44(3), pp. 605-614.
- [25] Kreplin, H., and Eckelmann, H., 1979, "Behavior of the Three Fluctuating Velocity Components in the Wall Region of a Turbulent Channel Flow," Phys. Fluids, 22(7), pp. 1233-1239.
- [26] Sumer, B. M., Arnskov, M. M., Christiansen, N., and Jorgensen, F. E., 1993, 'Tow-Component Hot-Film Probe for Measurements of Wall Shear Stress,' Exp. Fluids, 15(6), pp. 380–384.
- [27] McCroskey, W. J., and Durbin, E. J., 1972, "Flow Angle and Shear Stress Measurements Using Heated Films and Wires," ASME J. Basic Eng., 94(1), pp.
- [28] Savory, E., Gaudet, L., and Toy, N., 1995, "Laminar and Turbulent Shear Stress Measurement Using Surface Hot-Wire and Film Gauges," International Congress on Instrumentation in Aerospace Simulation Facilities, Wright-Patterson Air Force Base, OH, July 18-21, IEEE, New York, pp. 5.1-5.6.
- [29] Ho, C. M., and Tai, Y. C., 1998, "Micro-Electro-Mechanical-Systems (MEMS) and Fluid Flows," J. Fluid Mech., 30(1), pp. 579-612.
- [30] Mills, D. A., Chen, T. A., Horowitz, S., and Sheplak, M., 2019, "Development of a Differential Optical Wall Shear Stress Sensor for High-Temperature
- Applications," AIAA Scitech 2019 Forum, San Diego, CA, Jan. 7–11, p. 2112.
 [31] Eckelmann, H., 1974, "The Structure of the Viscous Sublayer and the Adjacent Wall Region in a Turbulent Channel Flow," J. Fluid Mech., 65(3), pp. 439–459.
- [32] Blackwelder, R. F., and Eckelmann, H., 1979, "Streamwise Vortices Associated With the Bursting Phenomenon," J. Fluid Mech., 94(3), pp. 577-594.
- [33] Kreplin, H., and Eckelmann, H., 1979, "Propagation of Perturbations in the Viscous Sublayer and Adjacent Wall Region," J. Fluid Mech., 95(2), pp. 305-322.
- [34] Alfredsson, P. H., Johansson, A. V., Haritonidis, J. H., and Eckelmann, H., 1988, "The Fluctuating Wall-Shear Stress and the Velocity Field in the Viscous Sublayer," Phys. Fluids, 31(5), pp. 1026-1033.
- [35] Wietrzak, A., and Lueptow, R. M., 1994, "Wall Shear Stress and Velocity in a Turbulent Axisymmetric Boundary Layer," J. Fluid Mech., 259, pp. 191–218.
- [36] Yang, J. M., Yoo, J. Y., and Choi, H., 1997, "Correlation of the Wall Skin-Friction and Streamwise Velocity Fluctuations in a Turbulent Boundary Layer (I). Analysis of Long-Time Averaged Space-Time Correlation," Trans. KSME B, 21, pp. 140-152.

- [37] Österlund, J. M., Lindgren, B., and Johansson, A. V., 2003, "Flow Structures in Zero Pressure-Gradient Turbulent Boundary Layers at High Reynolds Numbers," Eu. J. Mech. B, 22(4), pp. 379–390.
- [38] Kim, S., Ryu, S., and Yoo, J. Y., 2001, "Performance Characteristics of a V-Type Probe Developed for Wall Vorticity Measurement," Trans. KSME B, 25, pp. 514-522.
- [39] Ryu, S., Kim, S., and Yoo, J. Y., 2001, "Correlation of Wall Vorticity and Streamwise Velocity Fluctuations in a Turbulent Boundary Layer," Trans. KSME B, 25, pp. 523–532.
- [40] Preston, J., 1954, "The Determination of turbulent skin Friction by Means of Pitot Tubes," J. R. Aero. Soc., 58(518), pp. 109–121.
- [41] White, F. M., 1991, Viscous Fluid Flow, McGraw-Hill, New York.
- [42] Patel, V. C., 1965, "Calibration of the Preston Tube and Limitations on Its Use in Pressure Gradient," J. Fluid Mech., 23(01), pp. 185-208.
- [43] Champagne, F. H., Sleicher, C. A., and Wehrmann, O. H., 1967, "Turbulence Measurements With Inclined Hot-Wires Part 1. Heat Transfer Experiments With Inclined Hot-Wire," J. Fluid Mech., 28(1), pp. 153-175.
- [44] Hinze, J. O., 1975, Turbulence, McGraw-Hill, New York.
- [45] Yang, J. M., Yoo, J. Y., and Choi, H., 1997, "Correlation of the Wall Skin-Friction and Streamwise Velocity Fluctuations in a Turbulent Boundary Layer (II). Analysis of Conditionally Averaged Results," Trans. KSME B, 21, pp. 427-435.
- [46] Blackwelder, R. F., and Kaplan, R. E., 1976, "On the Wall Structure of the Turbulent Boundary Layer," J. Fluid Mech., 76(1), pp. 89-112.
- [47] Xi, L., and Graham, M. D., 2010, "Active and Hibernating Turbulence in Minimal Channel Flow of Newtonian and Polymeric Fluids," Phys. Rev. Lett., 104(21), p. 218301.
- [48] Xi, L., and Graham, M. D., 2012, "Intermittent Dynamics of Turbulence Hibernation in Newtonian and Viscoelastic Minimal Channel Flows," J. Fluid Mech., 693, pp. 433-472.
- [49] Whalley, R. D., Park, J. S., Kushwaha, A., Dennis, D. J., Graham, M. D., and Poole, R. J., 2017, "Low-Drag Events in Transitional Wall-Bounded Turbulence," Phys. Rev. Fluid., 2, p. 034602.
- Kushwaha, A., Park, J. S., and Graham, M. D., 2017, "Temporal and Spatial Intermittencies Within Channel Flow Turbulence Near Transition," Phys. Rev. Fluid., 2, p. 024603.
- [51] Park, J. S., Shekar, A., and Graham, M. D., 2018, "Bursting and Critical Layer Frequencies in Minimal Turbulent Dynamics and Connections to Exact Coherent States," Phys. Rev. Fluid., 3, p. 014611.
- [52] Murlis, J., Tsai, H. M., and Bradshaw, P., 1982, "The Structure of Turbulent Boundary Layers at Low Reynolds Numbers," J. Fluid Mech., 122(1), pp. 13-56.
- [53] Blackwelder, R. F., 1977, "On the Role of Phase Information in Conditional Sampling," Phys. Fluids, 20(10), pp. S232-242.
- [54] Johansson, A. V., Her, J., and Haritonidis, J. H., 1987, "On the Generation of High-Amplitude Wall-Pressure Peaks in Turbulent Boundary Layer and Spots,' J. Fluid Mech., 175(1), pp. 119–142.
- [55] Zilberman, M., Wygnanski, I., and Kaplan, R. E., 1977, "Transitional Boundary Layer Spot in a Fully Turbulent Environment," Phys. Fluids, 20(10), pp. S258-S271.
- [56] Sillero, J. A., Jiménez, J., and Moser, R. D., 2013, "One-Point Statistics for Turbulent Wall-Bounded Flows at Reynolds Numbers Up to $\delta^+ \approx 2000$," Phys. Fluids, 25(10), p. 105102.
- [57] Harun, Z., Monty, J. P., Mathis, R., and Marusic, I., 2013, "Pressure Gradient Effects on the Large-Scale Structure of Turbulnet Boundary Layers," J. Fluid Mech., 715, pp. 477–498.
- [58] Mochizuki, F. T., and Nieuwstadt, F. T. M., 1996, "Reynolds-Number-Dependence of the Maximum in the Streamwise Velocity Fluctuations in Wall Turbulence," Exp. Fluids, 21(3), pp. 218–226.
- [59] Jeon, S., Choi, H., Yoo, J. Y., and Moin, P., 1999, "Space-Time Characteristics of the Wall Shear-Stress Fluctuations in a low-Reynolds-Number Channel Flow," Phys. Fluids, 11(10), pp. 3084–3094.

 [60] Kim, J., Moin, P., and Moser, R., 1987, "Turbulence Statistics in Fully Devel-
- oped Channel Flow at Low Reynolds Number," J. Fluid Mech., 177, pp. 133-166.
- [61] Adrian, R. J., Meinhart, C. D., and Tomkins, C. D., 2000, "Vortex Organization in the Outer Region of the Turbulent Boundary Layer," J. Fluid Mech., 422, pp.
- [62] Subramanian, C. S., Rajagopalan, S., Antonia, R. A., and Chambers, A. J., 1982, "Comparison of Conditional Sampling and Averaging Techniques in a Turbulent Boundary Layer," J. Fluid Mech., 123, pp. 335–362.
- [63] Johansson, A. V., and Alfredsson, P. H., 1982, "On the Structure of Turbulent Channel Flow," J. Fluid Mech., 122(1), pp. 295-314.

Supplementary Information

Wall-shear-stress-based conditional sampling analysis of coherent structures in a turbulent boundary layer

Sangjin Ryu^{1,2}, Ethan Davis¹, Jae Sung Park¹, Haipeng Zhang¹, and Jung Yul Yoo³

¹Department of Mechanical and Materials Engineering, University of Nebraska-Lincoln, USA ²Nebraska Center for Materials and Nanoscience, University of Nebraska-Lincoln, USA ³Department of Mechanical Engineering, Seoul National University, Republic of Korea

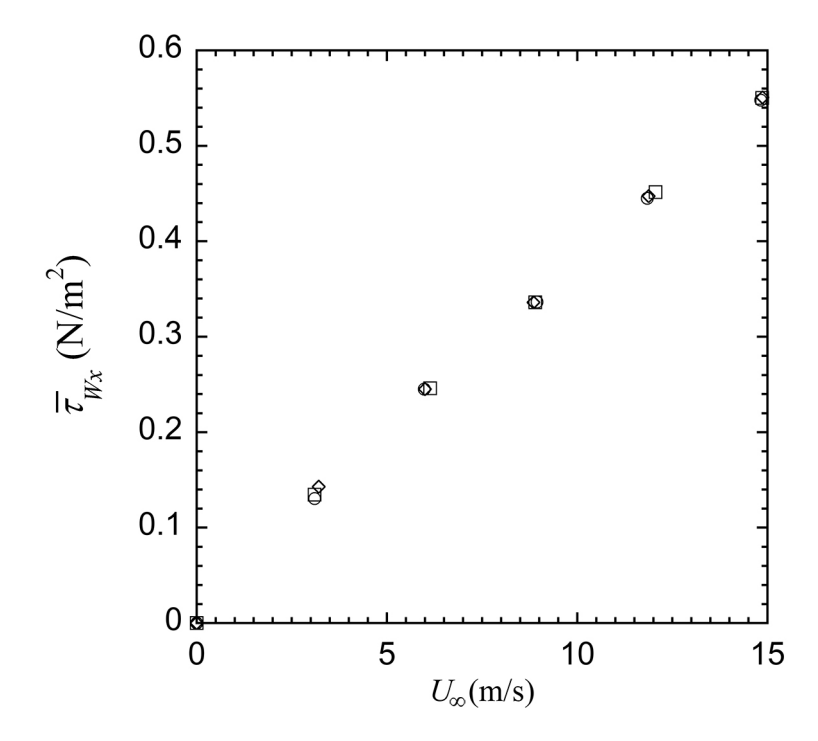


Figure S1. Streamwise wall shear stress ($\bar{\tau}_{Wx}$) measured using the Preston tube for the free stream velocity (U_{∞}) range of 0-14.9 m/s. The relative standard deviation (= standard deviation/mean; N = 3) ranged from 0.13% ($U_{\infty} = 8.9$ m/s.) to 9.22% ($U_{\infty} = 3.1$ m/s.).

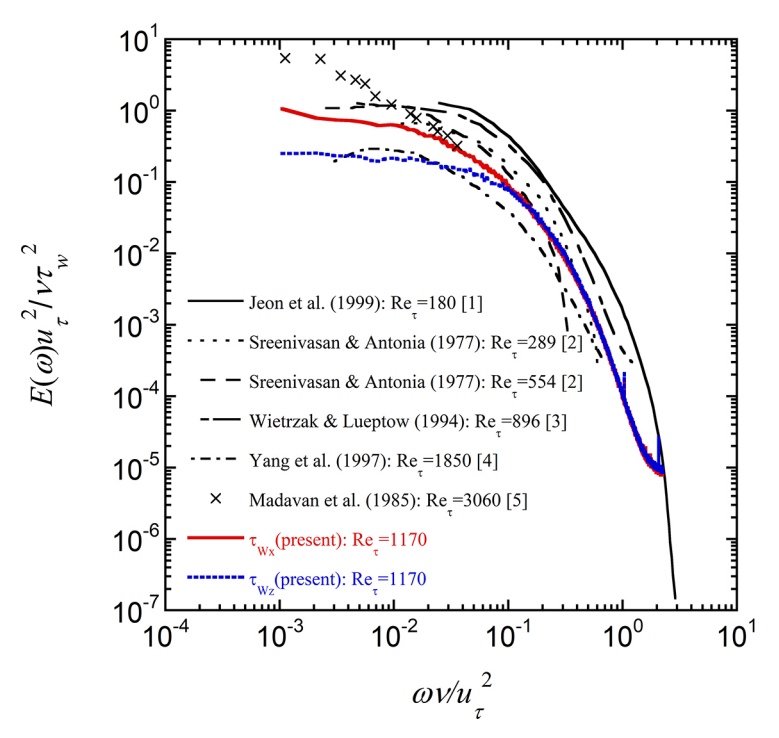


Figure S2. Energy spectrum of wall shear stress fluctuations [6].

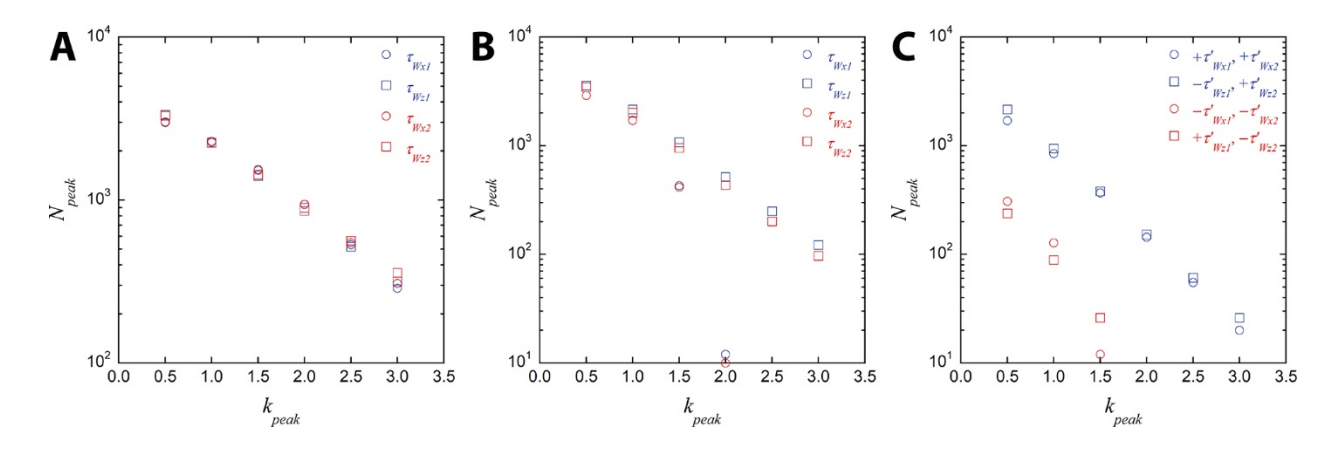


Figure S3. Effects of the peak detection threshold value (k_{peak}) on the number of detected peak events (N_{peak}). (A) Positive event. (B) Negative event. (C) Simultaneous event.

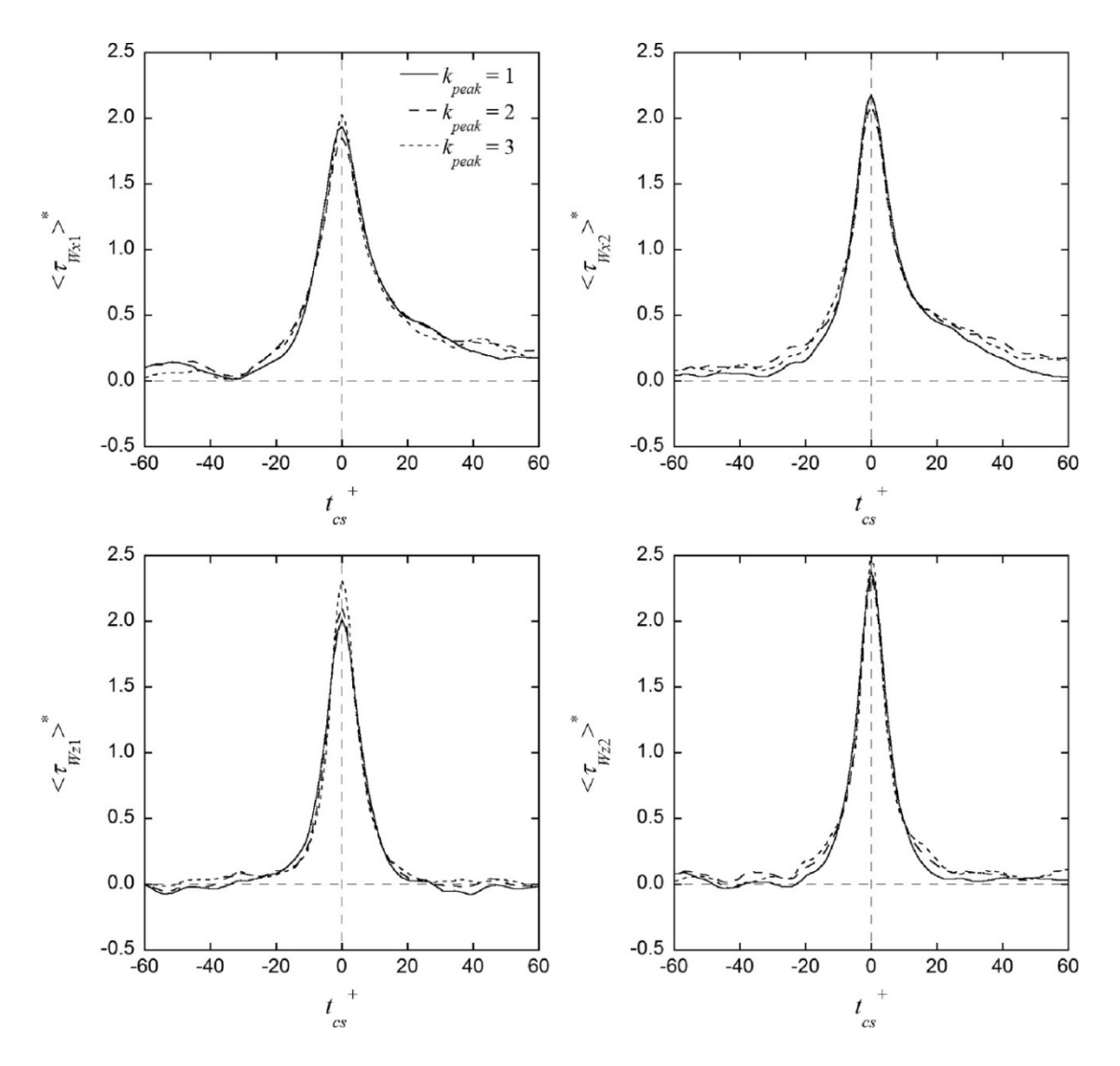


Figure S4. Effects of the peak detection threshold (k_{peak}) value on conditionally averaged wall shear stress.

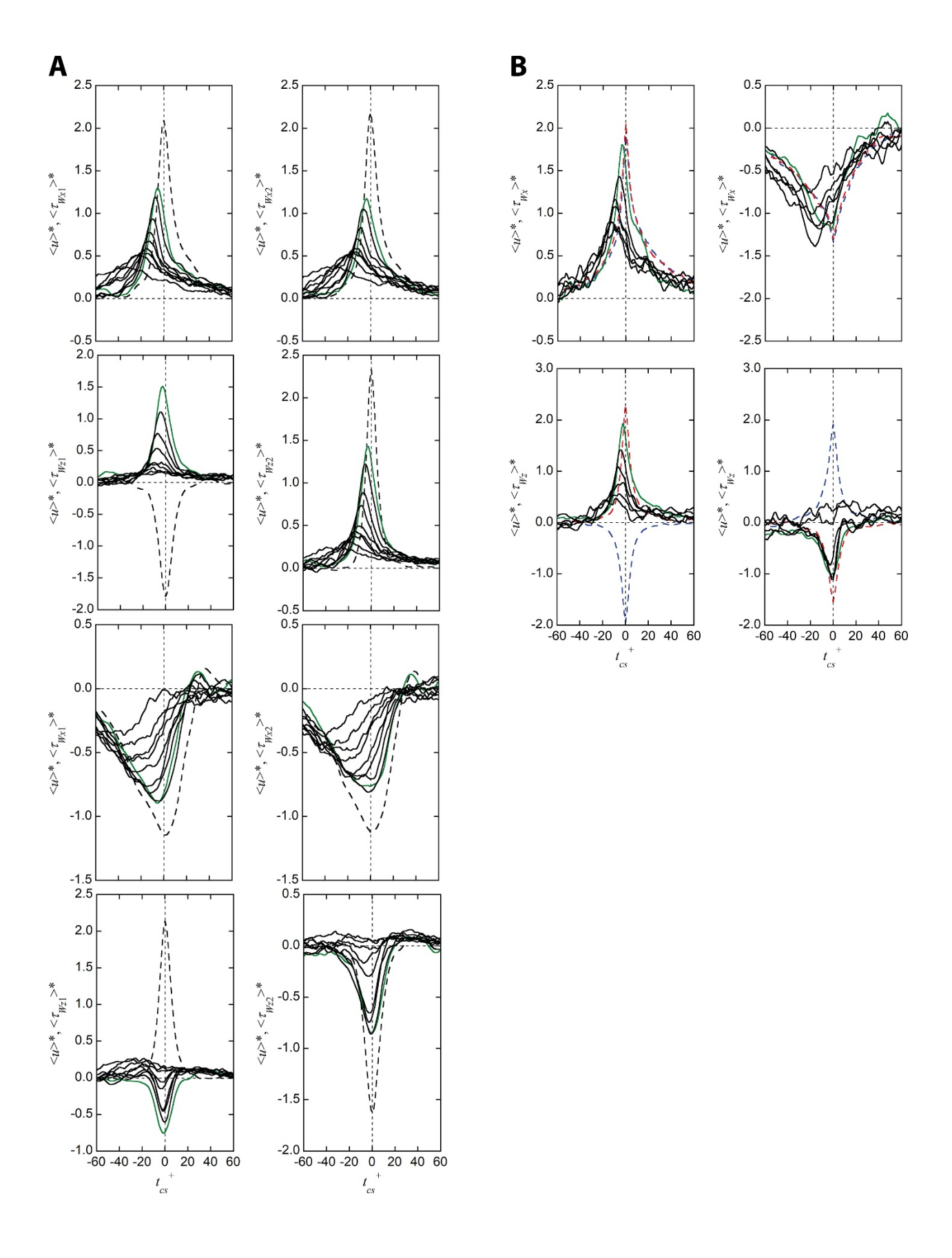


Figure S5. Conditionally averaged streamwise velocity fluctuations $\langle u \rangle^*$ with the peak events of wall shear stress $(k_{peak} = 1)$ with $\Delta x^+ = 0$. — : $\langle u \rangle^*$, -----: $\langle \tau_w \rangle^*$. The $\langle u \rangle^*$ curves of $y^+ = 7.3$ are shown in green, and y^+ increases in the order of 7.3, 10.5, 16.0, 21.3, 34.3, 51.8, 69.2, 103.9, and 173.5. (A) Peak events were detected using Probe 1 (left column) and Probe 2 (right column) separately. The top two rows are for sweep events, and the bottom two for burst. (B) Peak events were detected using the two probes simultaneously. Left column: Sweep events. Right column: Burst events.

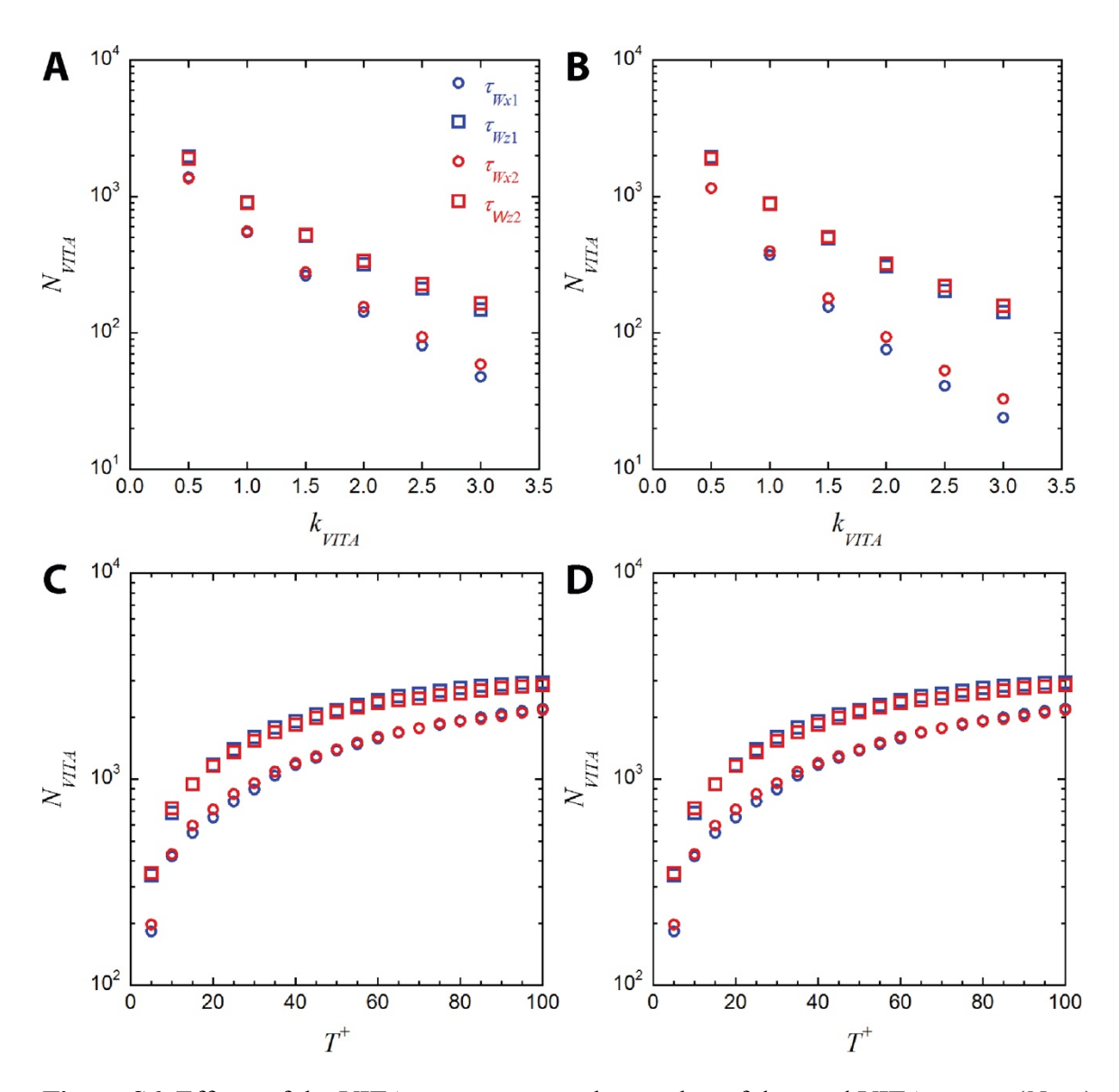


Figure S6. Effects of the VITA parameters on the number of detected VITA events (N_{VITA}). Effect of the threshold level (k_{VITA}) on N_{VITA} for (A) positive events and (B) negative events. A constant average time of $T^+ = 16$ was used. Effect of T^+ on N_{VITA} for (C) positive events and (D) negative events. $k_{VITA} = 1$ was used.

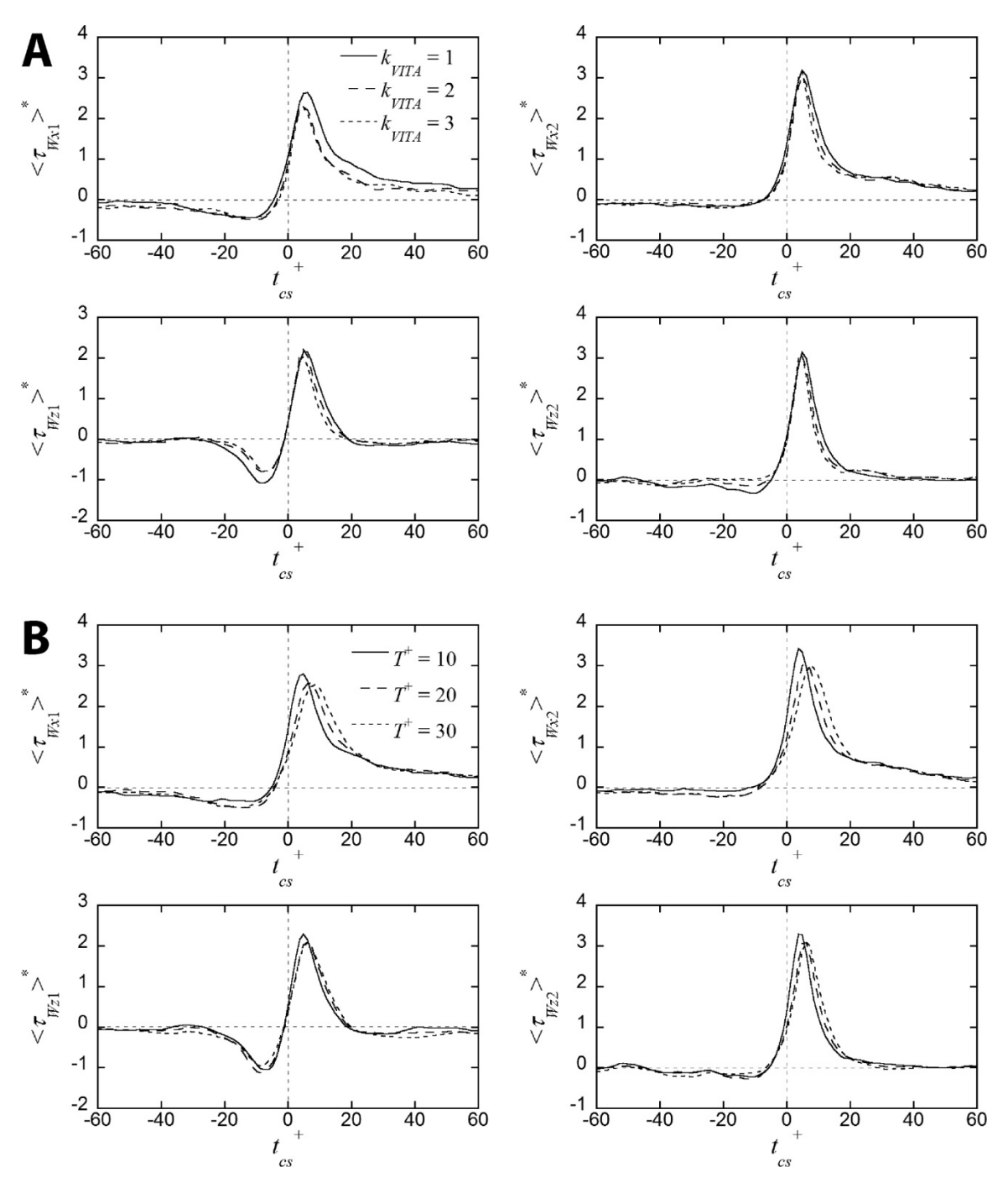
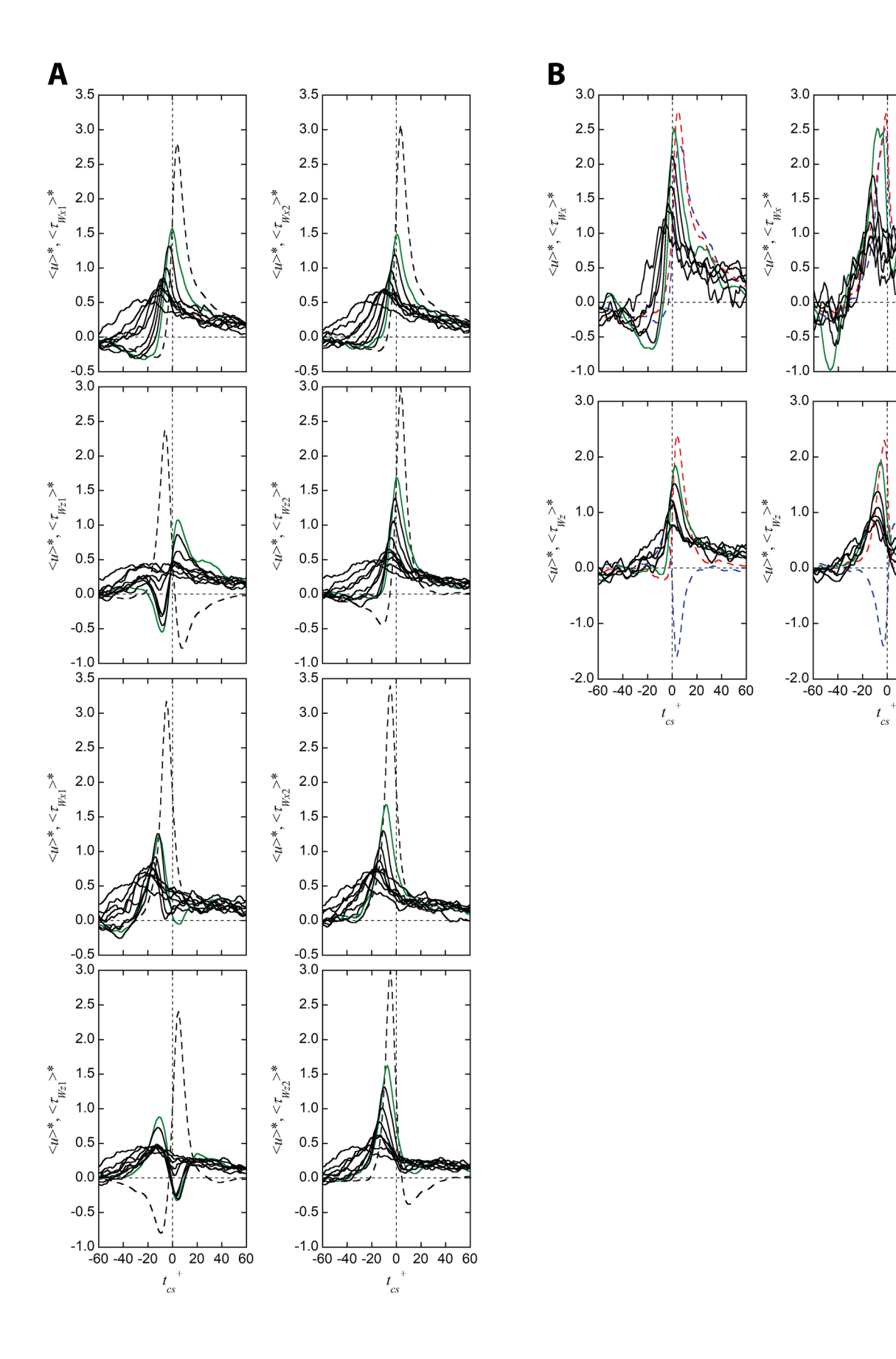


Figure S7. Effects of sampling parameters on conditionally averaged VITA events. (A) Effect of the threshold (k_{VITA}) level with $T^+ = 16$. (B) Effect of the averaging time (T^+) with $k_{VITA} = 1$.



20 40 60

 t_{cs}

Figure S8. Conditionally averaged streamwise velocity fluctuations $\langle u \rangle^*$ with the VITA events of wall shear stress ($k_{VITA} = 1$, $T^+ = 16$) with $\Delta x^+ = 0$. — : $\langle u \rangle^*$, -----: $\langle \tau_W \rangle^*$. The $\langle u \rangle^*$ curves of $y^+ = 7.3$ are shown in green, and y^+ increases in the order of 7.3, 10.5, 16.0, 21.3, 34.3, 51.8, 69.2, 103.9, and 173.5. (A) VITA events were detected using Probe 1 (left column) and Probe 2 (right column) separately. The top two rows are for sweep events, and the bottom two for burst. (B) VITA events were detected using the two probes simultaneously. Left column: Sweep events. Right column: Burst events.

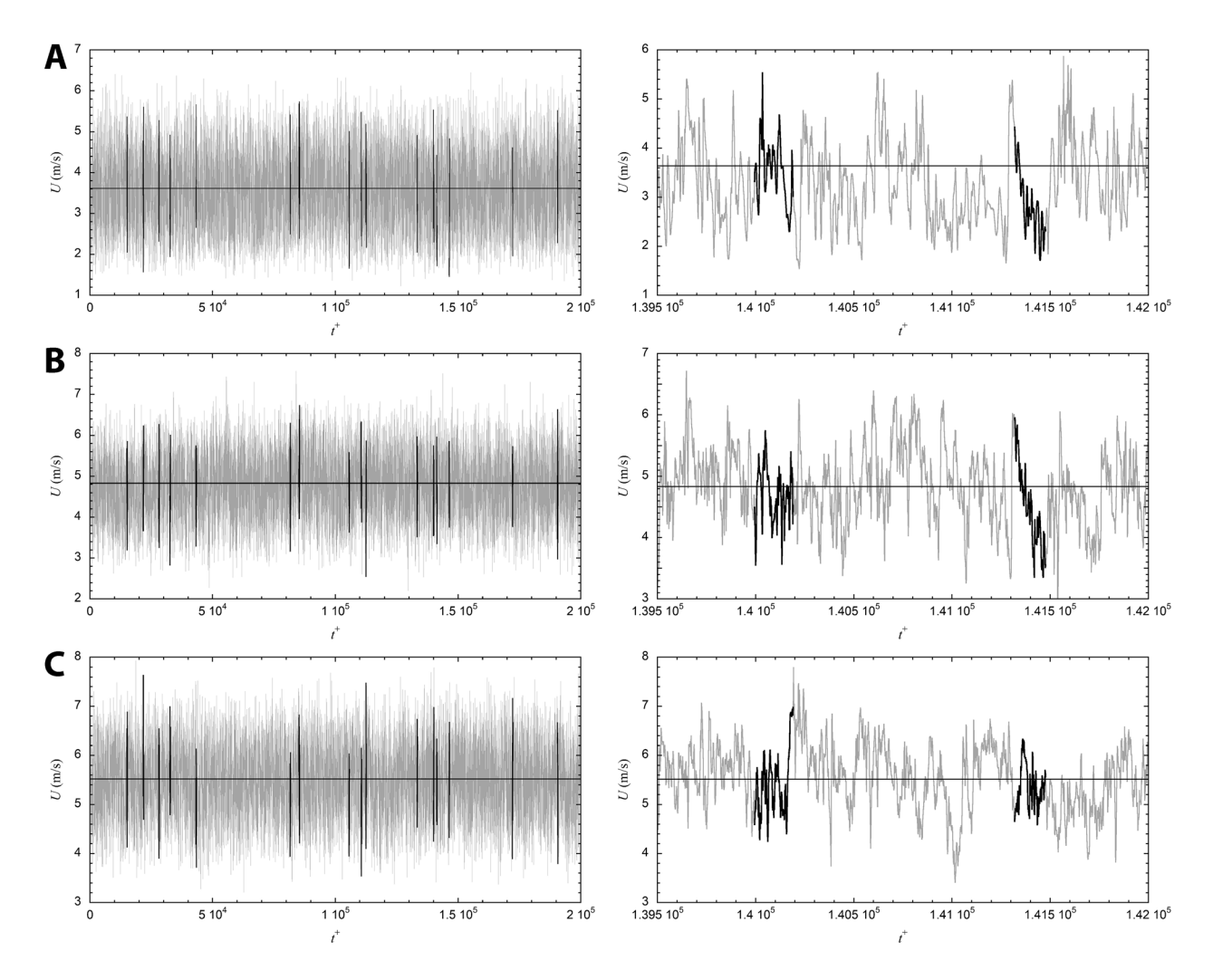


Figure S9. Temporal fluctuation of streamwise velocity (gray curve). Black curves correspond to the hibernating events shown in Fig. 10. The right column shows magnified plots as the inset of Fig. 10 shows. (A) $y^+ \approx 15$. (B) $y^+ \approx 50$. (C) $y^+ \approx 99$.

References

- [1] Jeon, S., Choi, H., Yoo, J. Y. and Moin, P. (1999) Space-time characteristics of the wall shear stress fluctuations in a low-Reynolds-number channel flow. *Phys. Fluids*, 11:3084-3094.
- [2] Sreenivasan, K. R. and Antonia, R. A. (1977) Properties of wall shear stress fluctuations in a turbulent duct flow. *J. Appl. Mech.*, 44:389-395.
- [3] Wietrzak, A. and Lueptow, R. M. (1994) Wall shear stress and velocity in a turbulent axisymmetric boundary layer. *J. Fluid Mech.*, 259:191-218.
- [4] Yang, J. M., Yoo, J. Y., and Choi, H. (1997) Correlation of the wall skin-friction and streamwise velocity fluctuations in a turbulent boundary layer (II). Analysis of conditionally averaged results. *Transactions of the KSME B*, 21:427-435.
- [5] Madavan, N. K., Deutsch, S. and Merkle, C. L. (1985) Measurements of local skin friction in a microbubble-modified turbulent boundary layer. *J. Fluid Mech.*, 156:237-256.
- [6] Kim, S., Ryu, S., and Yoo, J. Y. (2001) Performance characteristics of a V-type probe developed for wall vorticity measurement, *Transactions of the KSME B*, 25:514-522.